Degradation of ZnS:Cu,Au,Al phosphor powder and thin films under prolonged electron bombardment

by

Kenneth Thembela Hillie
(MSc)

A thesis submitted in fulfilment of the requirements for the degree

PHILOSOPHIAE DOCTOR

in the

Faculty of Natural and Agricultural Sciences
Department of Physics

at the

University of the Free State
Republic of South Africa

Promoter: Prof. H.C. Swart
Co-promoter: Prof. G.L.P. Berning

October 2001

This thesis is dedicated to the memory of the late

Prof. C.M. Demanet

as my mentor and later a valuable friend.

"For a successful technology, reality must take precedence over public relations, for Nature cannot be fooled." Richard P. Feynman.

Acknowledgements:

I am deeply indebted to the following people:

- *My wife Zou and son Mlibo for their constant support and understanding throughout the duration of my research, I owe this to them.*
- *Our parents, Ndzotho, Zola, Slush, Silos and the entire family for their support during this period.*
- *My promoter Prof. H.C. Swart for his professional leadership that made me grow as a research scientist and for his wisdom.*
- *Prof. G.L.P. Berning as being the former head of the department who allowed me to embark on these studies and also as my co-promoter for his professional suggestions.*
- *Prof. W.D. Roos for the informal discussions that made an impact.*
- *J.K.O. Asante for always willing to listen and to the entire Physics department staff who made the environment conducive.*
- *Drs. C. Curren and C. Theron of the NAC for their valuable input for thin film deposition and RBS analysis, respectively, and the assistantship I got from the NAC staff.*
- *Prof. S.S. Basson of the Chemistry department for the valuable discussions that we engaged on.*
- *Dr P.W.J. van Wyk of the electron microscopy unit UFS.*
- *The Unitra physics department staff for granting permission to use their AFM.*
- *The UFS Electronics and Instrumentation units staff for their prompt response when I experienced a problem.*

Lastly, I would also like to extend my gratitude to the following organisations for financially sponsoring the entire project and myself.

- *National Research Foundation (NRF)*
- *Deutscer Akademischer Austauschdienst/ DAAD scholarship (1998-2000) together with the German embassy in Pretoria.*

Abstract

Auger electron spectroscopy (AES) and cathodoluminescence (CL), both excited by the same electron beam, were used to monitor changes in surface composition and luminous efficiency during electron bombardment. ZnS:Cu,Al,Au phosphor powders and thin films were subjected to prolonged electron beam bombardment of varying beam energies and different electron beam current densities in two different (O_2 and CO_2) vacuum gas ambients. The thin film phosphors were grown on Si (100) substrates by using XeCl (308nm) pulsed laser deposition (PLD) method. X-ray diffraction (XRD) measurements revealed that ZnS (100) films were preferentially grown on a Si (100) substrate. The RBS results show that the growth rate, increased with an increase of the N_2 pressure in the deposition chamber during deposition.

Degradation on both the powder and the thin film phosphors was manifested by a non-luminescent ZnO layer that formed on the surface of the phosphor according to the electron stimulated surface chemical reactions (ESSCR) mechanism.

Lower current densities lead to a higher surface reaction rate, due to a lower local temperature beneath the beam, which resulted into a more severe CL degradation. A lower temperature beneath the electron beam may lead to an increase in the surface reaction rate due to the longer time spent by the adsorbed molecules on the surface, with a direct increase in the ESSCR probability. Low current densities would also lead to surface charging due to a lower electron conductivity of the phosphor resulting in an increase in the CL degradation rate due to band-bending.

In the studies conducted between room temperature and 310 ^oC, an increase in the temperature led to a decrease in the surface reaction rate due to a decrease in the mean surface lifetime of the oxygen molecules on the surface, with a direct decrease in the ESSCR probability. Without the presence of the electron beam no chemical reactions, up to 310 ^oC, occurred on the surface. Therefore, local heating due to the electron beam irradiation is not responsible for the chemical reactions on the ZnS phosphor surface. At -125 °C the degradation was controlled by the residual small amount of water vapour in the system that is frozen at this low temperature. The thermoluminescence (TL) curves of the phosphor powder before and after degradation showed the influence of the O substitutional atoms that are created during electron bombardment in an O_2 ambient. The O substitutional atoms acted as electron traps.

On the electron beam bombardment of thin film phosphors, the degradation was more severe under O_2 ambient compared to the same partial pressure of CO_2 during electron beam bombardment, which is attributed to the free energy of formation of ZnO from ZnS when these respective gases are used. The degradation rate also depended on the energy of the electron beam, decreasing with increasing beam energy. This was interpreted according to the ionisation energy cross-section profile. The CL brightness increased

exponentially with the increasing energy beam as more free carriers that will subsequently recombine yielding CL, are excited at higher beam energies.
The thin film phosphor was also subjected to the electron beam bombardment after the phosphor film was coated with a CdO film by using a chemical bath deposition (CBD) method. The surface reactions were electron beam stimulated, resulting in the desorption of both Cd and S from the surface which happened as soon as the surface adventitious C was depleted. Sulphur from the ZnS accumulated on the surface but was soon depleted as volatile SO_x compounds. The CdO was reduced by an electron beam assisted mechanism in the presence of non-reducible ZnO in the CdO-ZnO system as the Zn from the underlying ZnS layer emerged to the surface. The CL intensity degradation of the coated film showed a dependence on the surface composition. The intensity remained constant until the Cd was reduced on the surface before a slight decrease was observed. The effect of the CdO capping layer on the intensity of the phosphor was evident until the CdO eventually disintegrated.

Keywords

Phosphor: A wide band gap semiconductor that is intentionally doped with impurities to emit the desired frequency of light.

Luminescence: It is a phenomenon whereby the emission of light occurs in excess of thermal radiation.

Cathodoluminescence: Luminescence produced by electron beam irradiation.

Phosphor degradation: Reduction of the efficiency of a phosphor material through prolonged electron bombardment.

Table of Contents

Title page …… ***i***

Dedication…… ***ii***

Acknowledgement …… ***iv***

Abstract …… ***v***

Chapter 1 Introduction

1.1. Brief history of the display technology ……..… ***1***

1.1.1. Cathode ray tubes (CRTs) ……... ***1***

1.1.2 Liquid crystal displays (LCDs) ……. ***2***

1.1.3. Field emission displays (FEDs) ……..… ***3***

1.2. ZnS phosphor degradation literature review ……..... ***4***

1.3. The aim of this study …….. ***7***

1.4. The layout of the thesis ……..… ***8***

References ……. .. ***9***

Chapter 2 On the theory of luminescence processes of Zinc Sulphide (ZnS) based phosphor material

2.1. Introduction ……... ***11***

2.2. Energy transfer in the phosphors ……..... ***12***

2.3. Quenching of luminescence ……..… ***15***

2.3.1. Action of adventitious impurities "killers"…….. 15

2.3.2. Saturation…….. 16

2.3.3. Concentration quenching…….. 17

2.3.4. Thermal quenching…….. 17

2.4. Decay characteristics ……..... ***19***

2.5. Phosphor aging ……..... ***20***

2.6. Mathematical interpretation of the degradation …….. ***20***

References ……... ***23***

Chapter 3 Experimental techniques and procedures

Introduction ……... ***25***

3.1. Experimental techniques ……..……. ***25***

3.1.1. Auger Electron Spectroscopy (AES) ……..... 25

3.1.2. Scanning Electron Microscope (SEM)……..... 26

3.1.3. Atomic Force Microscope (AFM)…… 26

3.1.4. Rutherford Back-Scattering (RBS)…….…. 27

3.1.5. X-Ray Diffraction (XRD) ……..... 27

3.2. Experimental procedures……... 28

3.2.1. Current densities…….……..... 28

3.2.2. Temperature…….…..... 29

3.2.2.1. High temperature without sputtering.…….. 29

3.2.2.2. High temperature with sputtering.…….. 30

3.2.2.3. Low temperature.…….....… 30

3.2.3. Laser deposition…… 30

3.2.4. O_2 versus CO_2 on the degradation of a phosphor thin film…... 31

3.2.5. CdO coating on a thin phosphor film…….…..… 32

3.2.5.1. Deposition.…… 32

3.2.5.2. Coating.…… 32

3.2.5.3. Electron beam bombardment.…… 33

References……...…… 34

Chapter 4 The effect of current density on the degradation of the phosphor powder in an O_2 ambient

4.1. Introduction…….…..... 35

4.2. AES and CL for different current densities……...…..… 35

4.3. Conclusion……...… 41

References……...… 42

Chapter 5 The effect of temperature on the degradation of the phosphor powder in an O_2 ambient

5.1. Introduction…….. 43

5.2. AES and CL at different temperatures of the sample……..… 43

5.3. Conclusion……..….. 50

References……... 52

Chapter 6 Characterisation of ZnS thin films grown on Si (100) by XeCl pulsed laser ablation

6.1. Introduction……. 53

6.2. Characterisation…….. 54

6.3. Conclusion……..….. 59

References…….….. 60

Chapter 7 Electron beam induced degradation of a pulsed laser deposited ZnS:Cu,Au,Al thin film on a Si (100) substrate

7.1. Introduction…….…… 62

7.2. AES and CL analysis……..…..… 62

7.3. Conclusion…….….. 67

References…….…..…. 68

Chapter 8 The effect of CdO coating on the degradation of a ZnS thin film phosphor material

8.1. Introduction……..... 69

8.2. AES, CL, RBS, SEM and XRD analysis……..……..…… 70

8.3. Conclusion…….……...……... 75

References ……...….... 77

Chapter 9 Low temperature effect on the degradation of the ZnS phosphor powder

9.1. Introduction……...….. 78

9.2. AES and TL analysis……... 78

9.3. Conclusion……...…… 82

References……...… 83

Chapter 10 Conclusion and recommendations…… 84

APPENDIX…… 88

Calculations to predict the spontaneity of the reactions at any temperature by using the Gibbs-Helmholtz equation……. 88

LIST OF FIGURES…….….. 90

BIBLIOGRAPHY……... 91

Degrees…….. 91

Presentations in international conferences……...….. 91

Presentations in local conferences……... 91

Manuscripts appearing in conference proceedings……. 92

Publications in international journals……. 93

Chapter 1

Introduction

This chapter commences with the brief history of the display technology and puts more emphasis on the field emission display advantages over other specified display technologies. It then follows with the literature review on the phosphor material which is an important component of the emission display mechanism and on which the whole study is based. The chapter finishes by describing the aim of the study and the layout of the thesis.

1.1. Brief history of the display technology

Although there are also other available display technologies, this brief introduction will only focus on cathode ray tubes, liquid crystals and field emission displays as they have been and still surpass the other display technologies.

1.1.1. Cathode Ray Tubes (CRTs):

In 1897 Karl Ferdinand Braun made a breakthrough by the invention of the Cathode Ray Tube (CRT) scanning device [1] that was utilised for displaying electrical signals. Braun introduced a cathode-ray tube with a fluorescent screen, known as the cathode-ray oscilloscope. Kosma Zworykin [2] invented the cathode-ray tube called the kinescope in 1929, a tube needed for television transmission and Philo Farnsworth [3] invented the image dissector. The screen would emit visible light when struck by a beam of electrons. Phosphor screens using three beams of electrons have allowed CRTs to display millions of colours. This technological evolution later became the framework for information technology and a huge gain for home entertainment. Televisions, computers, automated teller machines, video game machines, monitors and radar displays all contain cathode-ray tubes. These CRT based display devices still render a role in our daily lives in the beginning of the 21st century and the multimedia infrastructure would not have immensely evolved had it not been for them. The problems associated with the CRTs though are the

inherent bulkiness due to the tube's design, the substantial weight and the high power needed for operation.

1.1.2. Liquid Crystal Displays (LCDs):

In the late sixties P.G. de Gennes [4] who later received a Nobel Prize in physics for his pioneering work, revisited the concept which was first introduced in the late thirties. It is about the phases that have the mechanical and the symmetry properties that are intermediate between those of a liquid and those of a crystal. For this reason they have often been called liquid crystals (LC). This is a state of matter, which is normally strongly anisotropic in some of its properties while retaining a certain degree of fluidity. Detailed investigations at describing their structures, the thermodynamic, optical and mechanical properties and their behaviour under external fields have been extensively undertaken over the years [4,5]. This information provided a platform for the anticipated realisation of compact technology and an inevitable move towards Flat Panel Displays (FPD). Digital display watches, portable calculators and recently, cell phones and laptop computer screens, manifested the development of liquid crystal display (LCD) based products. As with any technology there are parameters that have to be stretched to extremes to broaden the diversity in its utilisation and this is still the case with the LCD technology. In an attempt to prolong and improve the role of the LCDs, a number of flat panel displays technologies have been developed to assist in this regard [6]. The disappearing passive display is now being replaced by the active matrices liquid crystal displays (AMCLDs) using the thin film transistor (TFT) as the driving technology [7,8] and they are still a competitive force in the flat panel display market. However, none of these can compete with improved power, brightness efficiency, video response, viewing angle, operating temperature, packaging, full colour gamut, ruggedness and scalability which was predicted for field emission displays [9].

1.1.3. Field Emission Displays (FEDs):

The key elements of the FED system are: a cathode on which the emitter tips are fixed, an anode faceplate containing the phosphor pixels and spacers between the anode and cathode to support the structure against atmospheric pressure as illustrated in figure 1.1.

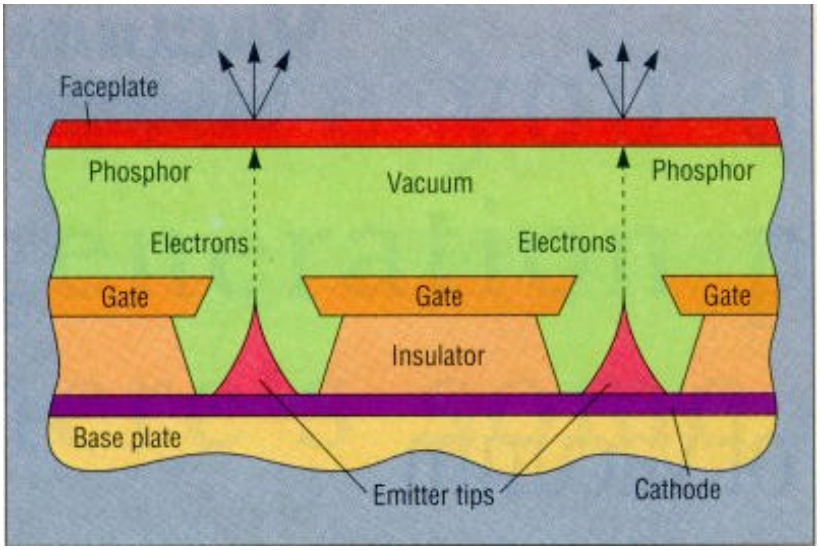

Figure 1.1 shows the cross-sectional view of the field emission cathodes (FED) [9].

It operates in an emissive mode just as the scanning electron beams of the CRT, for the cathodoluminescent excitation of the phosphors. Unlike the hot cathode in the CRT, the FEDs multitude of emitters form a planar addressable source of electrons fabricated so as to be on an aperture in a metal electrode that forms the gate (Spindt gate). Because of their potential to provide full-colour displays with CRT picture quality but with much reduced weight and bulk, FEDs are being aggressively developed by leading electronic companies (e.g. Candescent Technologies, Samsung etc.) worldwide. FEDs utilisation is in transportation, industry, consumer market, computers and business, which is in descending order of the projected market trends by the end of this decade, 2009 (www.samsung.co.kr).

In operation, electrons tunnel from the array of tips and are accelerated across a potential difference in a vacuum to strike the phosphor and emit light. The distance from the tip to the phosphor is determined by the trade-offs in the interrelation between the standoff voltage and the spacer shape, size and aspect ratio. To stand off 1 kV requires a gap of at least 200μm, and for a 5 kV potential a gap of at least 1 mm is needed [10]. The latter gap carries two consequences, one being that the electrons diverge sufficiently within that distance to require some form of active focussing which is an added design complexity and cost. The second being that the design of the internal support structure becomes difficult. The phosphors may be patterned to define the pixel, in which case three phosphors are deposited to achieve the primary colours of red, green and blue. Alternatively, a white phosphor may be used with an overlying, patterned set of thin-film filters to achieve the full colour display. These trade-offs and together with technology and materials choice [11] determine whether the product will be competitive in the market place.

Novel techniques for improving the performance of the FED have been embarked on. These include the improvements in the design of new FED structures [12], the synthesis and processing of new emitter arrays [13-16] and the development of new phosphors [17-19].

1.2. ZnS phosphor degradation literature review

The phosphor material forms the important part of the FED display technology since the light efficiency mostly depends on it. The phosphor is usually a wide band gap semiconductor that has been doped with impurities to modify the energy gap for appropriate light frequency output. The incentive in using conventional CRT phosphors is that they have shown high efficiency in converting electron beam energy into light [20]. Compared to ~10^{-9} Torr that the CRT usually operates in, the huge surface to volume ratio associated with the FED system introduces its own unique problems that affect the overall FED picture quality and operation.

The space between the phosphor and the emitter tip is small, consequently limiting the voltage to avoid arcing and dielectric failure. The low energy beam does not penetrate much into the phosphor resulting in the luminescence generation occurring close to the surface of the phosphor. Due to this shallow excitation depth, the condition of the phosphor surface is critical to the luminescence efficiency and since the surface is exposed to the impinging molecules of the residual gases, these gases play a significant role on the degradation of the luminescence. The residual gases are usually hydrogen, oxygen, carbon dioxide, water vapour, carbon monoxide, methane and other small traces of hydrocarbons and their partial pressures that appreciate in the FED vacuum environment.

Pfahnl [21] studied the degradation of several phosphors under electron bombardment and formulated the following Pfahnl law,

$$I = \frac{I_0}{(1 + CN)}, \tag{1}$$

where I is the aged intensity, I_0 is the initial intensity, N is the number of electrons deposited per square centimetre and C is the burn parameter that is equal to the inverse of the number of electrons per square centimetre required to reduce the intensity to half its original value. Pfahnl speculated that electron bombardment would result in a non-radiative transition through the creation of new recombination centres or the deactivation of an activator centre by changing its state of ionisation and also reported that the dependence of the rate of degradation of ZnO upon the vacuum pressure within a sealed CRT being more pronounced at higher pressures. Itoh *et al.* [22] showed that electron irradiation of the ZnS:Zn phosphor accelerated the formation of the sulphate on the phosphor surface in a H_2O vapour ambient and caused the evaporation of sulphide gases such as S, SO and SO_2 from the phosphor surface. This decomposition of the phosphor was enhanced by the dissociation of H_2O on the phosphor surface. Swart *et al.* [23-25] and Sebastian [26] extensively investigated ZnS phosphors under prolonged low energy (2 keV) electron beam bombardment at different experimental conditions for powdery and thin film materials, respectively. They postulated an electron beam stimulated surface chemical reaction (ESSCR) model that produces a non-luminescent layer on the surface of

the phosphor. Although the model is not entirely accountable for the luminescence reduction [25], there are proposed defect hypothesis that reconciles it [26,27].

For the ZnS phosphor under electron bombardment in a reactive gas ambient such as oxygen, the initiating event [28] could be the core level ionisation of Zn with the valence electrons of the Zn metal transferred to the S anion. Since no electrons are available to permit the relaxation of the core hole, an electron is then drawn from the S to permit relaxation of the core level by inter-atomic Auger cross transition. As electrons can be emitted from the S to carry away the excess energy involved in the Auger process, the S atom is left with a net positive charge surrounded by positive metal atoms. Concurrently as the data suggests, the electron beam dissociates the adsorbed reactive molecular species to reactive atomic species on the surface of the phosphor. A new compound of zinc and the resultant atomic reactive species will be formed on the surface of the phosphor through a surface chemical reaction and the volatile sulphur compounds will be released into the vacuum chamber. It is the newly formed layer that is non-luminescent that reduces the luminescence of the material. In the case of P22G phosphor in the oxygen environment, Oosthuizen *et al.* [28], proved that a ZnO layer was formed on the surface of the phosphor after electron bombardment with the subsequent release of SO_2 gas. In the space restricted environment associated with the FEDs the desorbed SO_2 gas might deposit on the emitters since they are very close to the phosphor making them inefficient. Seager *et al.* [29] also reported the influence of vacuum environment on the aging of phosphors at low electron energies.

Kingsley and Prener [30], after studying the CL intensity as a function of the accelerating potential for a number of ZnS:Cu phosphor powders each coated with a known thickness of a non-luminescent ZnS thin layer, deduced that the luminescent efficiency is dominated by the power loss of the electron beam in the non-luminescent coating. Greeff and Swart [31-33] used Monte Carlo calculations to simulate the degradation effects of the ZnO layer on ZnS. They also derived an expression to calculate a normalised value for the CL intensity using electron energy loss profiles generated by Monte Carlo. Using the CL quantification expression they simulated the curves relating the CL intensity to the ZnO thickness, and assuming that the diffusion interface was non-luminescent, the CL intensity

decreased as the thickness of the oxide and the width of the interface increased [34]. The calculated oxide thickness compared extremely well with experimental measurements.

Low voltage also requires an increase in the current of the beam so as to maintain the brightness intensity that is directly proportional to the beam power, P = IV, where I is electron beam current and V is the potential difference between the tip and the metal gate. An increase in the beam current may lead to saturation [35] and an increase in local temperature due to the electron beam, which both hinder the phosphor performance.

Another notable problem that impedes the phosphor performance is surface charging. Since the phosphor is usually a wide band gap material the negative charge from a low secondary electron emission coefficient might accumulate on the surface, as it can not be conducted away. The accumulated charge alters the surface potential, which in turn alters the kinetic energy of the primary electrons and also increases the probability that the electron-hole pair for the CL generation process will be swept apart before they radiatively recombine to emit light [36].

1.3. The aim of this study

In addition to the referred research in the cited articles and to understand the degradation of ZnS:Cu,Au,Al phosphor material subjected to the FED operational conditions, the following were investigated:

1. The effect of current density on the degradation of the phosphor powder in an O_2 ambient
2. The effect of temperature on the degradation of the phosphor powder in an O_2 ambient
3. The growth of XeCl pulsed laser deposited ZnS thin films on Si (100) substrates for CL

4. Electron beam induced degradation of the laser deposited phosphor film on a Si (100) substrate in an O_2 and a CO_2 ambient
5. The effect of a CdO coating on the degradation of a ZnS thin film in an O_2 gas ambient.

The results on the above topics culminated in six publications. These references are shown under the section on published material.

1.4. The layout of the thesis

This chapter serves as a prelude and summarises the background of the display technology and the incentive to embark on this study. It also highlights the research that has already been done on this particular phosphor material (ZnS:Cu,Au,Al) and outlines the research carried out in this thesis.

Chapter 2 deals with the theory of the light generation process by the ZnS:Cu,Au,Al phosphor, the luminescence quenching mechanism and the mathematical interpretation of the degradation model. In chapter 3, a brief description of the surface science analysis techniques that were used is given and the reasons for each specific choice are given. In chapter 3, the results on the effects of current density on the phosphor degradation in an O_2 ambient are discussed. The dependence of degradation on the temperature of the ZnS phosphor in an O_2 environment is discussed in chapter 5. In chapter 6, the characterisation of the XeCl pulsed laser deposited ZnS thin films is reported. The degradation of the thin film in both O_2 and CO_2 is discussed in chapter 7 and the effect of a CdO coating on the degradation of the film is discussed in chapter 8. Chapter 9 is the extension of Chapter 5 in which the results of the degradation of the phosphor powder at low temperature in O_2 environment are discussed

Chapter 10 contains the concluding remarks on the overall study with suggestions on future studies for the compatibility of the ZnS phosphors in the FED environment.

References:

[1] C.R. Stannard and B.B. Marsh, in *Cathode Ray Tube* (Ed. P.DiLavore, McGraw-Hill, New York, 1975).

[2] V.K. Zworykin U.S. Patent # 2, 141, 059 December 20, 1938.

[3] P.T. Fransworth, U.S. Patent # 1, 773, 980 August 26, 1930.

[4] P.G. de Gennes in *The physics of liquid crystals*, (Eds. W. Marshall and D.H. Wilkinson, Oxford university press) 1974.

[5] S. Chanddrasekhar in *Liquid crystals*, (Eds. M.M. Woolfson and J.M. Ziman, Cambridge university press, 1977)

[6] Y.R. Do and J.W. Bae, J. Appl. Phys., **88(8)** (2001) 4660.

[7] S. Naemura, in *Flat Panel Display Material II,* eds. (M.K. Hatalis, J. Kanicki, C.J. Summers and F. Funada), 1996, p 295.

[8] T. Tsukada, in *Flat Panel Display Material II,* eds. (M.K. Hatalis, J. Kanicki, C.J. Summers and F. Funada), 1996, p 3.

[9] P.H. Holloway, J. Sebastian, T. Trottier, H. Swart and R.O. Peterson, Solid State Technology, August (1995) 47.

[10] S.M. Jacobsen, Journal of SID, **4/4** (1996) 331.

[11] M.M.G. Slusarczuk, in *Flat Panel Display Material II,* eds. (M.K. Hatalis, J. Kanicki, C.J. Summers and F. Funada), 1996, p 363.

[12] S.J. Kwon, K.J. Hong, J.D. Lee, C.W. Oh, J.S. Yoo and Y.B. Kwon, J. Vac. Sci. Technol. **B 18(3)** (2000) 1227.

[13] R. Baptist, F. Bachelet and C. Constancias, J. Vac. Sci. Technol. **B 15(2)** (1997) 385.

[14] H.S. Uh, S.J. Kwon and J.D. Lee, J. Vac. Sci. Technol. **B 15(2)** (1997) 472.

[15] Y. Sohda, D.M. Tanenbaum, S.W. Turner and H.G. Craighead, J. Vac. Sci. Technol. **B 15(2)** (1997) 343.

[16] L. Nilsson, O. Gröning, P. Gröning, O. Küttel and L. Schlapbach, Thin Solid Films, **383** (2001) 78.

[17] B.K. Wagner, J. Penczek, S. Yang, F.-L. Zhang, C. Stoffers, C.J. Summers, P.N. Yocom and D. Zaremba, Proc. Intl. Display Research Conf., Sept. 15-19 (1997) Canada.

[18] M. Yokoyama and S-H. Yang, J. Vac. Sci. Technol. **A 18(15)** (2000) 2472.

[19] J-C. Park, H-K. Moon, D-K. Kim, S-H. Byeon, B-C. Kim and K-S. Suh, Appl. Phys. Lett. **77(14)** (2000) 2162.

[20] T. Hase, T. Kano, E. Nakazawa and H. Yamamoto, Advances in electronics and electrophysics, **79** (1990) 271.

[21] A. Pfahnl, in *Advances in Electron Tube Techniques* (Perganon, New York), (1961) 204.

[22] S. Itoh, T. Kimizuka and T. Tonegawa, J. Electrochem. Soc., **136 (6)** (1989) 1819.

[23] H.C. Swart, T.A. Trottier, J.S. Sebastian, S.L. Jones and P.H. Holloway, J. Appl. Phys., **83(9)** (1998) 1.

[24] H.C. Swart, L. Oosthuizen, P.H. Holloway and G.L.P. Berning, Surf. Interface. Anal., 26 (1998) 337.

[25] H.C. Swart, J.S. Sebastian, T.A. Trottier, S.L. Jones and P.H. Holloway, J. Vac. Sci. Technol., **A 14** (1996) 1697.

[26] J.S. Sebastian, PhD thesis, University of Florida, Florida, USA, 1998.

[27] C.W. Wang, T.J. Sheu, Y.K. Su, M. Yokoyama, Appl. Surf. Sci., **113/114** (1997) 709.

[28] L. Oosthuizen, H.C. Swart, P.E. Viljoen, P.H. Holloway and G.L.P. Berning, Appl. Surf. Sci., **120** (1997) 9.

[29] C.H. Seager, D.R. Tallant, L. Shea, K.R. Zavaldi, B. Gnade, P.H. Holloway, J.S. Bang, X.M. Zhang, A. Vecht, C.S. Gibbons, P. Trwoga, C. Summers, B. Wagner and J. Penczek, J. Vac. Sci. Technol. **A 17(6)** (1999) 3509.

[30] J.D. Kingsley and J.S. Prener, J. Appl. Phys., **43 (7**) (1972) 3073.

[31] A.P. Greeff and H.C. Swart, Surf. and Interface Anal., **29(12)** (2000) 807.

[32] A.P. Greeff and H.C. Swart, Surf. and Interface Anal., **31** (2001) 448.

[33] H.C. Swart and A.P. Greeff, Surf. and Interface Anal., Accepted October 2000.

[34] A.P. Greeff and H.C. Swart, Thin Solid Films, submitted.

[35] J.R. McColl, J. Electrochem. Soc.: Solid-State science and technology, **129(7)** (1982) 1546.

[36] H.C. Swart, A.P. Greeff, P.H. Holloway and G.L.P. Berning, Appl. Surf. Sci., **140(1-2)** (1999) 63.

Chapter 2

On the theory of luminescent processes of Zinc Sulphide (ZnS) based phosphor material

2.1. Introduction

A phosphor is a luminescent material fabricated from a wide-band gap material that is specifically doped with impurities for a particular wavelength emission. They are usually in the form of powders but in some cases, thin films. The impurities that are intentionally introduced to the material are referred to as activators and the material as the host or matrix. The host material should be transparent enough to enable the transfer of visible light to the surface of the phosphor. Different activators produce deep acceptor levels at distinct depths, which is the main cause for different emission colours of the phosphor. The phosphor material used in this study was commercially available zinc sulphide (ZnS) doped with Cu, Au as activators, and with Al as a co-activator (ZnS:Cu,Au,Al). This is a standard green luminous CRT phosphor numbered P22G with the Commission International del'Eclairage (CIE) standard colorimetric observer co-ordinates: x = 0.38, y = 0.608, with a wurtzite crystal structure and was obtained from Osrum Sylvania, USA. The P22G phosphor consisted of non-uniform particles with sizes ranging from 1.4µm to 4.5 µm.

In the sulphide phosphors, the emission can be greatly increased with a dopant of a IIIa or VIIa group that is referred to, as a "co-activator" but it has no influence on the emission colour. The co-activator produces a donor level that captures an electron that will then radiatively combine with a free hole captured in the deep acceptor levels, thereby emitting a photon whose energy is equal to the band gap minus the depth of the acceptor and donor levels. ZnS with an energy gap of 3.7 eV at 300K is a suitable host material for these phosphors, which have shown high efficiency and brightness under CRT applications [1].

2.2. Energy transfer in the phosphors

When a phosphor is bombarded by energetic electrons a multitude of free carriers (free electrons and free holes) are produced along the path of the incident electron. The electron-hole pair generation rate G (s^{-1}) for semiconductors is given by the following equation [2]

$$G = E_b I_b (1 - \eta_{bs}) / qE_{eh} . \quad (1)$$

Where E_b is the energy of the primary electron beam, I_b is the electron-beam current, E_{eh} is the average energy required to create an electron hole pair, q is the electronic charge and η_{bs} is the back-scattered electron coefficient that is dependent on the material and beam voltage. $E_{eh} = 2.8E_g + E'$, where 0.5 eV< E'< 1.0 eV. E' reflects phonon participation [3]. These free carriers will, depending on impurities and the defect nature of the host, recombine according to one of the luminescent transitions in Figure 2.1 [1].

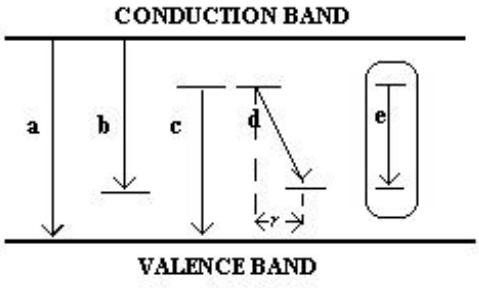

Figure 2.1 Models of electron transitions resulting in luminescence (a) From conduction band to a hole in the valence band; (b) from a conduction band to an acceptor level; (c) from a donor level to a hole in the valence band; (d) from a donor level to an acceptor level; (e) within a localised luminescent centre.

During the relaxation between characteristic energy levels of the solid, photons are produced that are detected as cathodoluminescence (CL). The P22G phosphor emission is due to the donor acceptor transition represented by (d) in Figure 2.1 [4]. It is a deep donor-acceptor pair (DAP) luminescence of the unlocalised extrinsic type [5]. This transition involves electrons and holes trapped on donor and acceptor levels respectively, which will either recombine radiatively through a DAP route or non-radiatively through deep level impurity route, see Figure 2.2. In the ground state of the system, both the donor and acceptor levels are ionised as a result of charge compensation provided by ion

substitution of Al^{3+}, Cu^{+} and Au^{+3} ions for Zn^{2+} ions. These ionised donor and acceptor levels rapidly capture free electrons and holes that have been produced by excitation, respectively, consequently being neutralised. Then, depending on the lifetime of these states, the captured electron at the donor will be transferred radiatively to the acceptor and recombine with the hole therein. Discrete shallow impurity luminescence is usually observed at low temperature (< -243 °C) because of thermal ionisation [6]. The schematic presentation of P22G is shown in Figure 2.2 below.

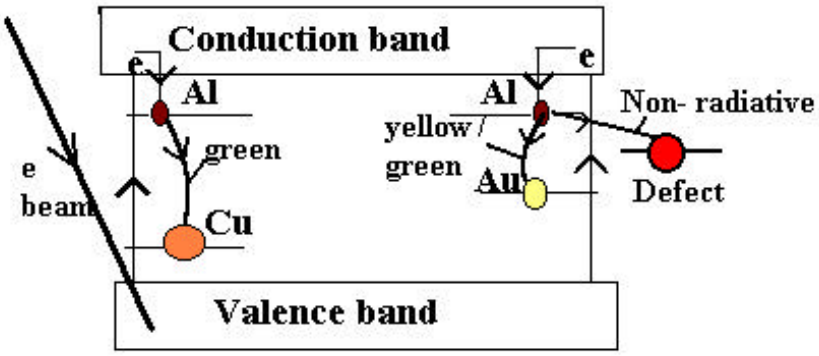

Figure 2.2 The schematic presentation of the luminescence process in ZnS:Cu,Al,Au phosphor

Cu and Au create different acceptor levels within the band gap of ZnS. This arrangement enables the phosphor to emit slightly different wavelengths through the aluminium co-activator dopant as shown in the diagram, Figure 2.2. Following are the three main features of the DAP emission mechanism. (1) The transition can occur in pairs with a wide range of intra-pair separation, if the depth of either donor or acceptor is sufficiently shallow. (2) The photon energy emitted by a DAP increases with decreasing pair separation. This feature is expressed by the following equation [7]

$$E_p(r) = E_g - (E_a + E_d) + \frac{q^2}{\varepsilon r} - \left(\frac{q^2 b^5}{\varepsilon r^6}\right). \qquad (2)$$

Where E_p(r) is the emitted photon energy, E_g is the band gap energy, E_a and E_d are the energy levels associated with isolated donor and acceptor, respectively, r is intra-pair separation, q is electronic charge, ε is the dielectric constant for the static field and b is an adjustable van der Waals parameter, $\frac{q^2}{\varepsilon r}$ represents the Coulomb interaction energy

between a DAP separated by distance *r*. The polarisation term (van der Waals energy for interacting dipoles) is represented by $\frac{q^2 b^5}{\varepsilon r^6}$. The last term in equation (2) is usually negligible except for very close pairs [7]. From equation (2) it can be seen that $E_p(r)$ shifts toward lower energies with increasing *r*. (3) The optical transition probability, *W(r)* of the pair emission also increases with decreasing intra-pair separation [4]. The probability is considered to be proportional to the square of the overlap of the donor and acceptor wave functions. The donor and acceptor are hydrogenic (the wave function decays exponentially with distance) and the spread of the donor is generally much larger than that of an acceptor. It is then enough to consider only the spread of the donor wave function in expressing the transition probability by

$$W(r) = W_0 \exp\left(\frac{-2r}{r_B}\right), \tag{3}$$

where W_0 is a constant and r_B is the Bohr radius of the donor state, even when the impurity states for which the effective mass approximation is not applicable (deep impurity) are involved.

Since the exited activator ions decay to the ground state by radiative and non-radiative transitions, if the decay of luminescence is exponential (see sections 1.4 and 1.6), then the total lifetime of the activator ions in the excited state, τ, is given by [8]

$$\tau^{-1} = \tau_r^{-1} + \tau_{nr}^{-1}, \tag{4}$$

where τ_r and τ_{nr} are the radiative and non-radiative lifetimes respectively. The quantum efficiency of the luminescence process in the activator ions, η_{act} is then given by

$$\eta_{act} = \frac{\tau_r^{-1}}{\tau_r^{-1} + \tau_{nr}^{-1}} = \frac{\tau}{\tau_r} \quad . \tag{5}$$

The external radiant efficiency, the ratio between the emitted optical flux and the absorbed input power can be given by the following equation [9],

$$\eta_{er} = (1 - \eta_{bs}) \frac{E_p}{E_{eh}} \eta_t \eta_{act} C_{extr} \, . \tag{6}$$

Where η_t is the quantum efficiency for the transfer of energy of electron-hole pairs to activator ions and C_{extr} is the average photon escape probability that accounts for the self-absorption of the luminescence and the other terms are as defined in the preceding equations. Degradation (the decrease of brightness with time under constant power) effects are due to changes in the phosphor and have an impact on the above parameters.

2.3. Quenching of luminescence

There are four dominant effects that reduce the phosphor efficiency and will be dealt with in the following subsections. These are the killers (an impurity when it reduces the intensity of the luminescence), brightness saturation, concentration quenching and thermal quenching.

2.3.1. Action of adventitious impurities " killers"

Any impurity or lattice defect can serve as a recombination centre if it is capable of receiving a carrier of one type and subsequently capturing the opposite type of carrier, hence annihilating the pair. Deep level impurities that are not intentionally introduced can capture free carriers produced by excitation during diffusion in competition with the luminescent centres causing them to recombine non-radiatvely [1]. Another type of killer action, that does not necessarily require free carriers for its quenching mechanism, removes energy away from the nearby luminescent centre by resonance energy transfer [10]. An iso-electronic trap is caused when an element belonging to the same column of the periodic table as that of the constituent atom of the semiconductor, is introduced and replaces a constituent atom. It can attract an electron or a hole because of the difference in electron affinity thereby becoming a killer [11]. Atoms and molecules adsorbed at the surface of the phosphor particles, defects that are inherent in the neighbourhood of a crystal surface, often become killers and may produce a "dead voltage layer". The formation of this non-luminescent layer discussed in Chapter 1, will also be discussed under the subsection 2.6 on the mathematical interpretation of the degradation model.

2.3.2. Saturation

Saturation occurs when the CL of the phosphors shows a sub-linear increase with an increase in the current density of the exciting electron beam. This effect is of utmost importance in the FED environment as the excessive decrease of the energy of the beam will result in the necessity to increase the current density to be able to maintain screen brightness. One of the major causes of brightness saturation is ground state depletion. Ground state depletion, which is to an extent concentration dependent, occurs when most of the centres are already in excited states leaving an insufficient number of available centres in the ground state to accept energy from excited carriers [12,13]. McColl [14] illustrated that the sub-linear response of (Zn,Cd)S:Cu,Al phosphor with increasing electron beam current density was due to an activator depletion mechanism which is more severe at low Cu concentrations (25-100 ppm) compared to medium concentrations (100-500 ppm). This drawback can be improved by choosing phosphors with an activator decay time (time lapsed before recombination from ionised levels) that is considerable less than the excitation dwell time (time by which the beam addresses the phosphor particle) [15]. In an attempt to qualitatively understand the luminescence saturation mechanism of ZnS:Cu,Al phosphor, Kuboniwa *et al.* [16], studied the excitation current density dependence of the luminescence efficiencies and decays at several activator concentrations, temperatures and accelerating voltages. They found that non-radiative deactivation of the luminescent centres occurs in the early stages of the decay, neither temperature nor the accelerating voltage effects the saturation and that saturation behaviour is independent of the Cu and Al concentrations in the region > 10^{-4} g.atom/mol-ZnS. The Auger recombination involving a donor-acceptor pair was postulated as the non-radiative process responsible for saturation. The Auger effect is a non-radiative process of a DAP due to the energy transfer to a third ("killer") centre (e.g., another donor level), followed by its ionisation. Thermal quenching due to the electron beam may also cause the saturation of luminescence at high current densities.

2.3.3. Concentration quenching

Aggregation of activator atoms at high concentration may change a fraction of the activators to killers because of the local field disturbance and induce the quenching effect due to resonance energy transfer [1]. Hoshina and Kawai [17], investigated the DAP recombination luminescence in ZnS:M,Al (M=Cu, Ag and Au) under cathode ray at room temperature and argued that the dominant non-radiative path for the DAP luminescence involves Auger recombination between an excited DAP and an ionised acceptor. They also highlighted the importance of the resonant energy transfer from the excited DAP to an interstitial Cu or Ag centre since this centre produces a broad absorption band over the entire visible wavelength. Zakrzewski and Godlewski [18] proved that Auger-type energy transfer process may limit considerably the CL quantum yield for heavily doped ZnS based phosphors under high excitation and hence deserves to be included when discussing the concentration quenching and energy transfer of the DAP emission intensity.

2.3.4. Thermal quenching

Increasing the temperature results in a reduction in light output due to thermal quenching. It occurs at high temperatures when the thermal vibrations of the atoms surrounding the luminescent centre transfer the energy away from the centre resulting in a non-radiative recombination, and the subsequent depletion of the excess energy as phonons in the lattice. By simplification, for the displacements of the interacting atoms in their individual co-ordinates, a generalised co-ordinate that represents all atoms can be applied in a configuration co-ordinate diagram [1] in Figure 2.3. In the diagram (Figure 2.3) the minima of the two curves 0 and A representing the ground and excited states, respectively, do not correspond since the stable configuration of the interacting atoms will be different for both states. With electron bombardment the system will be excited from point 0 to B and immediately adapts by changing the atomic configuration from B to the new equilibrium A along U_e with excess energy lost as heat.

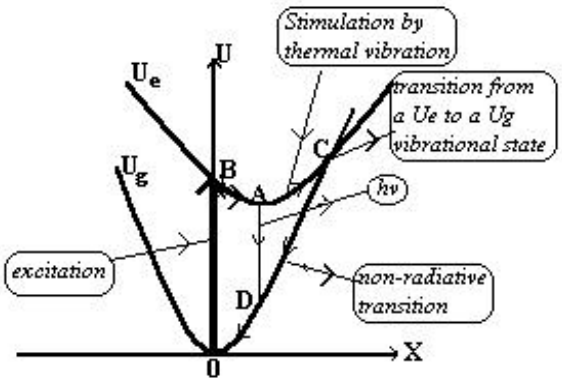

Figure 2.3 Configuration co-ordinate model of a luminescent centre. The potential energy of a luminescent centre is presented as a function of a generalised co-ordinate x with the parabolas, U_g and U_e, corresponding to the ground and excited states, respectively.

From this point the system can either undergo a radiative jump from A to D followed by a heat dissipating shift from D back to 0, or the stimulation by heat absorption of the centre from A to C along U_e at higher temperatures. With the increasing temperature, vibrational levels in the excited state are exacerbated, stimulating the transition from of the centre A to C. Since the process from A to C results from thermal stimulation, the probability of the non-radiative transition, *W(nr)*, is equal to the thermal activation probability W_{TA}, represented as [1]

$$W(nr) = W_{TA} = s\exp\left(\frac{-E_{AC}}{kT}\right). \tag{7}$$

Where the activation energy E_{AC} is the difference of potential energy between the points A and C, *s* is a frequency factor and *k* the Boltzmann constant. If *W(r)* is the probability of radiative transition, then the temperature dependence of the luminescence efficiency is given by

$$\eta = \frac{W(r)}{(W(r)+W(nr))} = \frac{W(r)}{\left(W(r)+s\exp\left(\frac{-E_{AC}}{kT}\right)\right)}. \tag{8}$$

The efficiency always decreases with increasing temperature, starting from some temperature *(T)* where the extreme right term of equation (7) becomes appreciable as compared with *W(r)*, and the luminescence eventually disappears.

The configuration co-ordinate model mostly applies on localised donors and is highly influenced by the deep acceptor-donor luminescence. In DAP luminescence one pair is regarded as one localised centre to which the configuration co-ordinate model is applied.

2.4. Decay characteristics

In the absence of traps, excited charge carriers are directly captured by recombination centres, and if only one kind of luminescent centre is present, the emission intensity decays exponentially with time as given by equation (9) with decay time constant equal to the lifetime τ of the centre [1].

$$I(t) \propto \exp\left(\frac{-t}{\boldsymbol{t}}\right). \tag{9}$$

The spectrum of the DAP emission is composed of many lines or bands, each of which corresponds to discrete separated pairs with a different decay rate as represented by equation (3). Therefore, the decay of the total emission is given by the sum of equation (9) for all pairs and will no longer follow the exponential law. Era *et al.* [19] observed decays of the DAP emission of ZnS:Cu,Cl(Al) and ZnS:Ag, Cl to follow a time power law,

$$I(t) \propto t^{-n}, \tag{10}$$

with an exponent n = 1.1-1.3 and that the decay becomes faster with increasing photon energy in the emission band. If the traps are present the decay becomes temperature dependent as the electrons can be thermally released to the conduction band and the luminescence will be prolonged by time the electrons spend in the traps. The time for the carrier to remain in such a trap, t_T , which depends on the probability of escape is given by,

$$t_T = s^{-1} \exp\left(\frac{E_T}{kT}\right), \tag{11}$$

where E_T is the depth of the trap to the conduction band. Assuming that the traps present in the phosphor are of a single depth and that the electrons released from the traps go directly to the luminescent centre without being recaptured, then the decay of the

luminescence follows the exponential function in equation (9) with the time constant equal to t_T [1].

2.5. Phosphor aging

During the course of operation, bombarded areas of the phosphor tend to become more or less darkened and degraded in efficiency with the aged portion usually turning black. This phenomenon is generally called "aging". Aging is not a new problem but has become a more serious predicament with the increasing demand for high current density operation required in FED to maintain brightness at low electron beam energies. The photolysis of ZnS phosphor that results from the simultaneous action of water vapour and short-wave UV radiation was reported many years ago [20]. During the process fine particles of metallic zinc separate locally on the surface of the sulphide causing the darkening of the material and due to this the luminescence properties of the phosphor change. Sviszt [20] asserted that the nature of the activator has a strong influence on the factors determining the darkening sensitivity of the phosphor and due to this on the decrease of the luminescence, too. Wang *et al.* [11] reported that the degradation mechanism of ZnS:Mn is mainly due to deep electron traps, which comes from the Mn activators reacting with surface water molecules. This trap behaves like a non-radiative centre resulting in poor brightness characteristics when samples become aged.

2.6. Mathematical interpretation of the degradation model (see Introduction)

To develop a mathematical model of ESSCR for the ZnS based phosphor, it is assumed that the rate of removal of S correlates with the decay of the CL intensity and that the concentration C_S can be modelled by a standard chemical reaction. Then the rate of change of the surface concentration, C_S can be expressed as [21]

$$\frac{dC_S}{dt} = -k' C_{as} C_s, \qquad (12)$$

where k' is a chemical rate constant that depends on the activation energy of the chemical reaction and C_{as} is the concentration of the adsorbed atomic species that will react with

the ZnS. The value of k' typically increases exponentially with an increase in temperature. The concentration of the adsorbed atomic species is:

$$C_{as} = N\sigma_{ma} n_a J \tau_{as}, \tag{13}$$

where N is the number of reactive atomic species produced from the parent molecule and depends upon the composition of the gases, σ_{ma} is the dissociation cross section of the molecules to atoms (which is a function of electron energy and current density [22]), n_a the surface population of the adsorbed molecules per square centimetre, J is the electron flux density (electrons $cm^{-2}s^{-1}$), and τ_{as} is the lifetime of a reactive atomic species, which is assumed to be very short. It is assumed that the rate of production of adsorbed atomic species limit the ESSCR reaction rate.

The surface population of the adsorbed molecules per square centimetre (n_a) can be expressed as

$$n_a = s\ I_{imp} \tau_a \tag{14}$$

where s is the sticking coefficient, I_{imp} the molecular impingement rate and τ_a the mean surface lifetime of a molecule. Substituting expressions for I and τ_a into Equation (14) leads to

$$n_a = s\left(\frac{P}{(2\pi mkT)^{1/2}}\right)\left(\tau_0 \exp\left(\frac{\Delta H_{des}}{kT}\right)\right) \tag{15}$$

where P is the partial pressure of the molecular gas, m the molecular mass, T is the temperature, k is the Boltzmann's constant, τ_0 is a combination of the molecular partition functions of the system in the equilibrium and activated states and the vibration frequency of the crystal lattice, and H_{des} is the desorption energy [23]. Substituting Equations (13) and (15) into (12) leads to

$$\frac{dC_S}{dt} = -k' C_S N \sigma_{ma} J \tau_{as} s\left(\frac{P}{(2\pi mkT)^{1/2}}\right)\left(\tau_0 \exp\left(\frac{\Delta H_{des}}{kT}\right)\right). \tag{16}$$

Equation (16) may be written as

$$\frac{dC_S}{C_S} = -KJPdt, \tag{17}$$

where K is defined by

$$K = k's N f_{ma} t_{as} \left(\frac{1}{(2pmkT)^{1/2}} \right) \left(t_0 \exp\left(\frac{\Delta H_{des}}{kT} \right) \right). \quad (18)$$

Integrating equation (17) with respect to time yields

$$C_S = C_S^0 \exp(-KPJt), \quad (19)$$

where the boundary condition $C_S = C_S(0)$ at time equal to zero was applied. *Jt* is the current density multiplied by time and is equal to charge per unit area, often-called Coulomb dose. This model predicts that the concentration of S will decrease exponentially with the Coulomb dose, and the rate of loss will be larger at higher gas pressures.

In this thesis the effect of current density and temperature on this degradation mechanism will be investigated. The influence of different reactive gas species in ambience during electron beam bombardment will be studied by comparing CO_2 and O_2 gas species. The phosphor material will also be coated by a CdO transparent conductive oxide barrier in an attempt to avoid degradation.

References:

[1] T. Hase, T. Kano, E. Nakazawa and H. Yamamoto, Advances in electronics and electrophysics, **79** (1990) 271.

[2] S.M. Davidson, J. Microscopy, **110** (1977) 177.

[3] C.A. Klein, J. App. Phys., **39** (1968) 2029.

[4] K. Era, S. Shinoya and Y. Washizawa J. Phys. Chem. Solids, **29** (1968) 1827.

[5] S. Shionoya, in *Luminescence of Solids* Ed. D.R. Vij (Plenum Press, New York), 1998, p95.

[6] S. Myhajlenko, in *Luminescence of Solids* Ed. D.R. Vij (Plenum Press, New York), 1998, p135.

[7] P.J. Dean, Trans. Mettal. Soc. AIME, **242** (1968) 384.

[8] D.B.M. Klaassen and D.M. de Leeuw and T. Welker, J. Lumin., **37** (1987) 21.

[9] D.J. Robbins, J. Electrochem. Society **127** (1980) 2694.

[10] D. Dexter, J. Chem. Phys. **21** (1953) 836.

[11] C.W. Wang, T.J. Sheu, Y.K. Su, M. Yokoyama, Appl. Surf. Sci., **113/114** (1997) 709.

[12] D.M. de Leeuw and G.W.'t Hooft, J. Lumin., **28** (1983) 275.

[13] R.Raue, M. Shiiki, H. Matsukiyo, H. Toyama and H. Yamamoto, J. Appl. Phys. **75 (1)** (1994) 481.

[14] J.R. McColl, J. Electrochem. Soc.: Solid-state Science and Technology, **129 (7)** (1982) 1546.

[15] C. Stoffers, S. Yang, F. Zang, S. M. Jacobson, B.K. Wagner and C.J. Summers, Appl. Phys. Lett., **71 (13)** (1997) 1759.

[16] S. Kuboniwa, H. Kawai and T. Hoshina, Jpn. J. Appl. Phys., **19 (9)** (1980) 1647.

[17] T. Hoshina and H. Kawai, J. Lumin., **12/13** (1976) 453.

[18] A. Zakrzewski and M. Godlewski, Appl. Surf. Sci., **50** (1991) 257.

[19] K. Era, S. Shinoya and Y. Washizawa J. Phys. Chem. Solids, **29** (1968) 1843.

[20] P. Sviszt, Phys. Stat. Sol., **(a) 4** (1971) k113.

[21] P.H. Holloway, J. Sebastian, T. Trottier, S Jones, X,-M. Zhang, J.-S. Bang, B. Abrams, W.J. Thomes and T.-J. Kim, J. Appl. Phys., **88 (1)** (2000) 483.

[22] H.C. Swart, L. Oosthuizen, P.H. Holloway and G.L.P. Berning, *Surf. Interface Anal*., **26 (5)** (1998) 337.
[23] J.B. Hudson, *Surface Science: An Introduction*. Butterworth-Heinemann, Boston, (1992) 179.

Chapter 3

Experimental techniques and procedures

Introduction

In this chapter a brief description of the instrumentation used in this study and more importantly the reason behind their preference will be given. Some of the techniques have been excessively utilised for surface interface studies and the method of data extraction has been put to test. These techniques are: Auger Electron Spectroscopy, Scanning Electron Microscope, Atomic Force microscope, Rutherford Back-Scattering Spectroscopy and the X-Ray Diffraction technique.
This will be followed by detailed experimental procedures that were followed for each topic delegated to a specific chapter.

3.1. Experimental techniques

3.1.1. Auger Electron Spectroscopy (AES)

As indicated in the introductory chapter, the CL generation occurs close to the surface of the phosphor, the surface chemistry therefore dramatically influences the efficiency of the phosphor. Auger electron spectroscopy, which is capable of identifying individual elements and with a shallow depth of about five monolayers from which data is taken [1], is particularly suited for surface analysis.

In the Auger process, the high-energy primary electron hits and liberates a core level electron thereupon ionising the atom. For this atom to reorganise itself to a lower energy state, an electron from the higher level will drop to the lower level to fill the void caused by the liberated electron. The surplus energy released in this transition is either emitted as a photon or given to another electron in the higher level. If the energy is sufficient, this electron can be ejected from the surface and detected as an Auger secondary electron.

Due to the specific energy levels involved in the transition and the energy of the detected Auger electron, the atom from which the electron was ejected can be identified. The changes in the chemical composition of the surface during degradation are thus easily monitored with the Auger electron spectroscopy.

With the use of an incorporated ion gun into the vacuum system, the Auger can also be utilised for depth profiling. As the ion gun etches away the material, the electron probe focused on the same spot can give information about the changes in element concentration with sputter depth. Depth profiling was employed on the thin film phosphor to identify the elements into the bulk of the material.

3.1.2. Scanning Electron Microscope (SEM)

The scanning electron microscope designed for studying the surfaces of conducting and semi-conducting materials directly [2], utilises a beam of focused electrons as an electron probe that is scanned in a regular manner over the specimen. The action of the electron beam stimulates the emission of the secondary electrons from the surface of the specimen, which are amplified to modulate the brightness of a display CRT that has its line scan driven in synchronism with the probe beam in the microscope column. There is a point by point correspondence between the brightness of each point in the display tube and the number of secondary electrons emitted from any point on the surface of the specimen. In this way, a two dimensional picture of the surface topography of the specimen is built up.

The SEM was utilised to acquire the surface images of the ZnS:Cu,Au,Al thin film and the CdO coated ZnS:Cu,Au,Al thin film.

3.1.3. Atomic Force Microscope (AFM)

The AFM, which was invented in the late 1980's is a versatile technique that produces three-dimensional (3D) renditions of the topographic features and makes it possible for the determination of the root-mean-square roughness (R_{rms}) of both conducting and non-

conduction surfaces [3]. In operation, a sharp tip (r~10nm) is put to the close approximation of the sample that is mounted on a piezoelectric scanner or a sample is put close to the tip mounted on the scanner. As the tip approaches the sample, the atoms in its apex will experience a repulsive force from the outermost atoms on the surface of the sample. In contact mode AFM, while the tip is scanning the sample or the sample scanning the tip in the x-y plane, an electronic feedback loop is enabled to maintain the constant repulsive force between the tip and the sample. This gives a 3D image of the surface topography. With the 3D information at atomic resolution, the R_{rms} of the surface can be calculated.

The AFM was used to measure the evolving surface morphology of the excimer laser deposited thin films.

3.1.4. Rutherford Back-Scattering (RBS)

RBS [4] characterises a quantitative depth of elements in a layer stack. Monoenergetic He^+ ions with energies 1 to 4 MeV impinge on the sample, and the energy of the backscattered ions is detected. This energy is characteristic of the mass and depth of the target atom. As a result, the area density and composition of the film is determined. With an independent thickness measurement the volume density can be calculated as well.

The RBS was suitably utilised for the material chemical composition and the thickness measurements of the ZnS phosphor thin films.

3.1.5. X-Ray Diffraction (XRD)

XRD technique has been extensively used over the years to determine the crystal orientation of film and powdered material. The atomic structure of the crystal is deduced from the way it diffracts a beam of X-rays in different directions. When a beam of monochromatic X-rays strikes a crystal, the wavelets scattered by the atoms in each plane combine to form a reflected wave. If the path difference for waves reflected by successive planes is a whole number of wavelengths, the wave trains will combine to produce a strong reflected beam. In geometric terms, if the spacing between the reflecting planes is

d and the glancing angle of the incident X-ray beam is θ then the path difference of the waves reflected by successive planes is $2d \sin \theta$. Hence the condition for diffraction is $n\lambda = 2d \sin \theta$, where n is an integer and λ is the wavelength of the X-ray [5].
In this study we used the XRD to determine the crystal orientation of the ZnS target before ablation, the ZnS films on Si (100) and the CdO film on a glass substrate.

3.2. Experimental procedures

In all the degradation experiments the Auger primary beam was used to bombard the sample, produce the secondary Auger electrons and to excite the CL.

The Auger measurements were made in a UHV chamber with a PHI Model 549 system and the spectra were recorded in the first derivative form with a modulation voltage of 4 V peak to peak. The phosphor powder and thin films were excited for CL measurements by the same primary electron beam that was used for Auger excitation. The electron beam size was stable during each experiment and the beam current variation was less than 2% during any particular experiment. The electron beam energy was 2 keV for all the Auger measurements, unless stated otherwise. CL measurements were done on the emitted light at an angle of 90^o to the incident electron beam. The CL data were collected through a quartz port and by using a Spectra Pritchard Photometer.
For all the XeCl pulsed laser deposition experiments, a Lamda-physik EMG 203MSE XeCl laser with a wavelength of 308 nm was used. Prior to deposition of the thin films, the Si (100) substrates were degreased in a sequential five-minute heated ultrasonic baths of acetone, methanol and isopropanol [6] and blow-dried with N_2 gas.

3.2.1. Current densities

The results obtained when the phosphor powder was subjected to electron bombardment with different electron current densities are shown in Chapter 4. The beam current densities were varied from 2.5 to 88 mA/cm^2. The experiments were done at an oxygen pressure of 1×10^{-6} Torr.

3.2.2. Temperature

The results obtained when the phosphor powder was subjected to electron bombardment at different temperatures are shown in Chapters 5 and 9. For these studies a sample holder with a resistive heating element for higher temperatures was used and a cooling stage for lower temperatures was utilised. The alumina and chromel thermocouples were imbedded on the copper sample holders that had the holes holding the powder. The cross sectional schematics of the heating (a) and cooling (b) set-ups used in the annealing and cooling experiments are presented in Figure 3.1 (a) and (b), respectively.

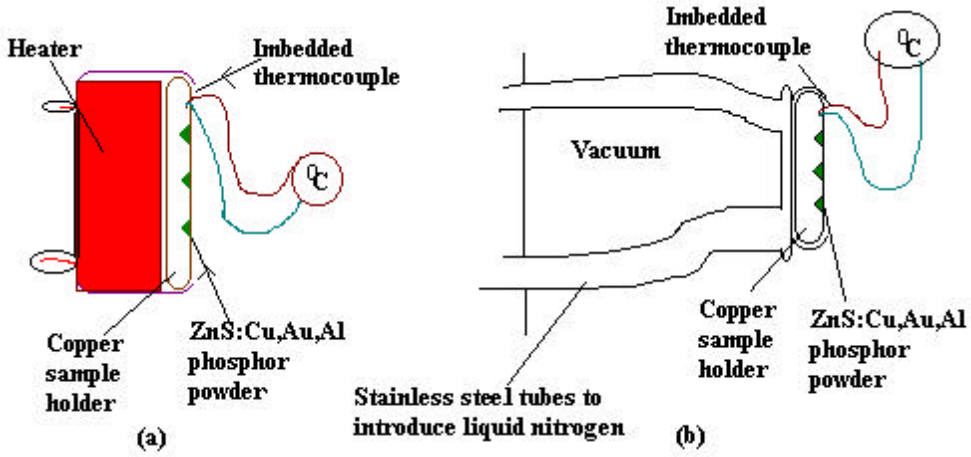

Figure 3.1 The cross sectional schematics of the heating (a) and cooling (b) set-ups.

3.2.2.1. High temperature without sputtering

In the *first set* of experiments the ZnS powder was annealed at temperatures between room temperature and 300 ^{o}C using the set-up illustrated in Figure 3.1 (a). The surface was not sputter-cleaned prior to electron irradiation for this set of experiments since Swart *et al.* [7] have shown that sputtering permanently degrades the luminescence efficiency of the ZnS phosphor. The experiments were done at an oxygen pressure of 2 x 10^{-6} Torr with an electron beam that had a current density of 88mA/cm^2.

3.2.2.2. High Temperature with sputtering

In the *second set* of experiments the sample surfaces were sputter-cleaned before the degradation process was started to make sure the initial conditions for each experiment were exactly the same, without any influence of the adventitious atmospheric C contamination. CL data was not collected due to the damage caused by the sputtering. A differential pumped ion gun (Perkin Elmer model (04-303A) was used for the Ar^+ ion sputtering. The Ar pressure in the ion gun was 5×10^{-5} Torr. The angle between the direction of the incident ion beam and the normal to the surface was 40^o. A 2 keV ion beam with ion current density of 22 $\mu A/cm^2$ was used for the sputtering. The sample was sputtered clean at each temperature (from room temperature up to 310 ^oC). The oxygen was introduced at 2 x 10^{-6} Torr while Auger measurements were done.

3.2.2.3. Low temperature

In the *third set* of experiments (Chapter 9) the phosphor powder was cooled to –125 ^oC by cold nitrogen gas obtained by evaporating liquid nitrogen, using the apparatus illustrated in Figure 3.1(b). In some experiments the liquid nitrogen cryogenic pump was used to verify the effect of the residual water vapour. This was achieved by introducing liquid nitrogen into the panels that run inside the system that are designed to freeze some residual gases on them to decrease the vacuum pressure. The phosphor was then subjected to electron beam with a current density of 8.7 mA/cm^2 at 2 x 10^{-6} Torr O_2 ambient. The surface compositional changes and the CL intensity were monitored during electron beam bombardment. Thermoluminescence (TL) glow curves were also monitored using a Spectra Pritchard Photometer.

3.2.3. Laser deposition

In chapter 6, the crystal structure and surface roughness of ablated ZnS phosphors on Si (100) were investigated by comparing four samples of ZnS based phosphors that were deposited on the silicon substrates with and without an inert gas in the deposition chamber. Auger electron spectroscopy (AES), X-ray diffraction (XRD), Rutherford back

scattering (RBS) and Atomic force microscopy (AFM) were utilised for the characterisation of the thin films.

The powder was grinded, then annealed for 3 h at 300 °C at a base pressure of 10^{-5} Torr, to evaporate the excess water for mechanical stability under pressure, and cold pressed by applying 15.5 x10^{8} Pa on a 1.27 cm diameter dye. The growth process was carried out in a vacuum chamber with base pressure of 10^{-5} Torr. The laser pulse energy was approximately 123 mJ and the repetition rate used was 10 Hz. A target to substrate distance of 3.5 cm was used. The deposition was carried out at substrate temperatures between 150 °C and 250 °C. Some of the samples were ablated at 10^{-5} Torr and others at a N_2 partial pressure of 10^{-3} Torr. The number of pulses was kept constant except for one sample where the pulses were doubled. The chemical composition of the topmost surface and the thickness of the films were obtained by UHV AES system and by RBS, respectively. A Perkin Elmer Model 04-303A differential ion gun incorporated in the UHV system with an argon ion source operated at a sputtering rate of approximately 1.3 Å per second was used for in-depth film investigations.

Film crystallinity was examined with a powder X-ray diffractrometer using CuK_{α} radiation. AFM measurements were carried out ex situ in ambient using a Park Scientific Autoprobe CP equipped with an AFM/LFM head operated in contact mode. A V-shaped Si_3Ni_4 cantilevers ('Microlever') of nominal force constant 0.03 Nm^{-1} with a sharpened tip of nominal radius 20 nm was used. The 3µm high tip is square pyramidal in geometry with a pyramidal apex semi-angle of 35°. The sharpened apex, however, has a semi-angle of 18°. Root-mean-square (rms) roughness (R_{rms}) values were determined from the AFM images using the PSI software. For statistical reasons and reproducibility the images were acquired on different regions of the sample.

3.2.4. O_2 versus CO_2 on the degradation of a phosphor thin film

A ZnS:Cu,Au,Al thin film that was deposited using XeCl pulsed laser at a substrate temperature of 200 °C for 6000 laser pulses (as explained above) was bombarded by an electron beam that had energies from 1 to 5 keV (see Chapter 7). The electron beam size was stable during each experiment but varied with each beam energy setting. The

experiments were done at an O_2 and CO_2 pressure of 5 x 10^{-7} Torr. The phosphor film was excited for CL measurements by the same primary electron beam that was used for Auger excitation, which had a beam current density of 16.1 mA/cm^2. When excited by the electron beam the thin films emitted a green luminescence, λ ~ 501 nm. Rutherford back scattering (RBS) was used to measure the thickness of the film.

3.2.5. CdO coating on a thin phosphor film

The experimental procedure for Chapter 8 has three sections that are: (a) deposition of the ZnS thin film by a pulsed laser, (b) coating of the film with CdO using the chemical bath deposition method and (c) bombardment of the sample with the electron beam to monitor the changes in surface composition and the CL efficiency.

3.2.5.1. Deposition

A ZnS:Cu,Au,Al film was deposited on Si (100) substrates by a XeCl pulsed laser deposition method of a commercially available powder that was pressed to form a pellet. The deposition process was carried out in a vacuum chamber with base pressure of 1.5 x 10^{-4} Torr, which was backfilled with N_2 to 10^{-2} Torr. The laser pulse energy was ~ 102 mJ and the repetition rate used was 10 Hz. A target to substrate distance of 4 cm was used and the deposition was performed at a Si(100) substrate temperature of 200 °C for 6000 laser pulses. The thickness of the film and the approximation of the stiochiometry were measured by the Rutherford back scattering.

3.2.5.2. Coating

The chemical bath deposition [8] was achieved by mixing 60ml of 0.04 M CdCl2 solution with 20ml of an ammonia solution 25% by weight. The solution was heated to 45°C. The ZnS:Cu,Au,Al thin film was inserted vertically into the solution. 0.125 ml of a 30% H_2O_2 solution was added into the solution at this temperature. The temperature was controlled between 45 °C and 50 °C throughout the 10 minutes deposition time. The deposition time was measured from the instant that the peroxide was poured into the heated solution.

The overall chemical reaction [9] for the formation of $Cd(O_2)_{0.88}(OH)_{0.24}$ can be written as shown in equation (1)

$$[Cd(NH_3)_6](OH)_2 + 0.88\ H_2O_2 \rightarrow Cd(O_2)_{0.88}\ (OH)_{0.24} + 1.76\ H_2O + 6NH_3 \qquad (1).$$

After the deposition the thin layers were immediately put into a furnace for oxidation. CdO films were prepared by annealing $Cd(O_2)_{0.88}(OH)_{0.24}$ thin films for 10 minutes at 200°C in a nitrogen atmosphere. The existence of covalent peroxides of Zn and Cd has been known for quite a long time [10,11] and the insolubility of these peroxides in ammoniacal solution is primarily the reason why such formation can be deposited on the phosphor surface. $Cd(O_2)_{0.88}(OH)_{0.24}$ films were transformed into CdO films according to the following reaction,

$$Cd(O_2)_{0.88}(OH)_{0.24} \rightarrow CdO + 0.44\ O_2 + 0.12\ H_2O. \qquad (2)$$

The thickness of the CdO film on the ZnS film was measured through a sputter depth profile using a Perkin Elmer Model 04-303A differential ion gun that is incorporated in the UHV system with an argon ion source operated at a sputtering rate of approximately 1.3 $Å s^{-1}$.

3.2.5.3. Electron beam bombardment

The CdO coated ZnS:Cu,Au,Al thin films were subjected to electron bombardment with an electron beam of 2 keV beam energy and a current density of 16.1 mA/cm^2 at an oxygen pressure of $5x10^{-7}$ Torr. The coated phosphor film was excited for CL measurements by the same primary beam that was used for Auger excitation. When excited by the electron beam the CdO coated phosphor films emitted a green luminescence. The CL measurements were made on the emitted light. The degradation of the CdO coated ZnS:Cu,Au,Al was compared to the uncoated ZnS:Cu,Au,Al thin film.

References:

[1] C.C. Chang, Surf. Sci. **25** (1971) 53.

[2] J. Davidson, J. Microsc. **110** (1977) 177.

[3] G. Binning, C.F. Quate and Ch. Gerber, Phys. Rev. Lett. **56**(9) (1986) 309.

[4] Handbook of Modern Ion Beam Materials Analysis, Eds. J.R.Tesmer and M.Nastasi, MRS Pittsburg 1995.

[5] L. Bragg, Scientific American, July (1968).

[6] J.M. Nel, K.T. Hillie, C.M. Demanet, F.D. Auret, H.L. Gaiger, Appl. Surf. Sci. **134** (1998) 22.

[7] H.C Swart, J.S. Sebastian, T.A. Trottier, S.L. Jones and P.H. Holloway, J. Vac. Sci. Technol. **A 14** (1996) 1697.

[8] M. Ortega-López, A. Morales-Acvedo and Bokhimi, Revista Mexicana de Física **42(5)** (1996) 776.

[9] M.Z. Nadjoski, I.S. Grozdanov and B. Minceva-Sukarova, J. Mater. Chem., **6(5)** (1996) 761.

[10] J.W. Mellor in *Inorganic and Theoretical Chemistry: A comprehensive Treatise*, (Longmans, Green & Co., 1946), p. 532.

[11] F.A. Cotton, G. Wilkinson, C.A. Murillo and M. Bochmann in *Advanced Inorganic Chemistry 6th Edition*, (John Wiley & Sons, New York, 1999), p. 460.

Chapter 4

The effect of current density on the degradation of the phosphor powder in an O_2 ambient

4.1. Introduction

The reduction of the Cathodoluminescence (CL) intensity was shown to depend exponentially on Coulomb loading (i.e. C/cm^2), on partial pressure of gas, and on the primary electron beam voltage [1,2]. Although the interactive constants (measure of the probability of surface reaction) and CL burning parameters (measure of the probability of CL degradation per incident electron) calculated from data collected at different current densities (45 to 58 mA/cm^2) were within experimental error the same [2], the variation in electron flux, however, was too small to really compare. The results from different laboratories show that there is a big difference in the degradation rate of the CL of ZnS phosphors degraded at lower current densities in comparison with the degradation in CL at higher current densities.

In this chapter Auger electron spectroscopy (AES) and CL, both excited by the same electron beam were used to monitor changes in surface composition and luminous efficiency of ZnS:Cu,Al,Au phosphor during electron bombardment with different electron current densities.

4.2. AES and CL for different current densities

The change in CL intensity and Auger Peak to Peak Heights (APPHs) of S, C, O and Zn for the ZnS:Cu,Al,Au phosphor versus Coulomb dose during electron bombardment, at an oxygen pressure of 1×10^{-6} Torr and a current density of 88 mA/cm^2, is shown in Figure 4.1.

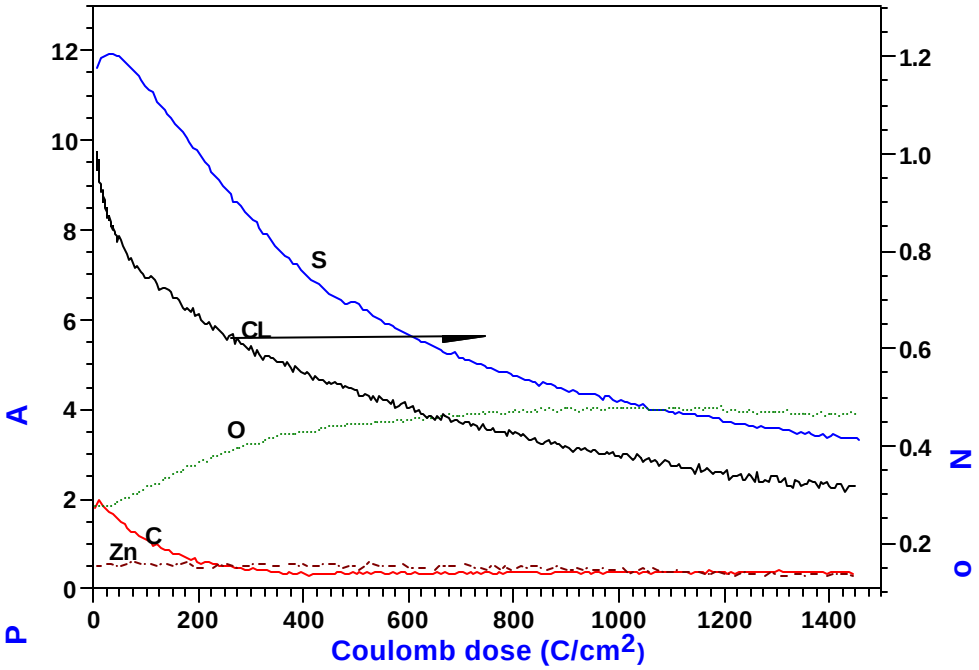

Figure 4.1 The APPHs of S, C, O and Zn as well as the CL measured at a current density of 88 mA/cm^{-2} as a function of Coulomb dose.

During electron bombardment both the C and S signals decrease exponentially. Concurrent with the decrease in C and S signals the O peak signal increased. This was proved to be due to the formation of a ZnO surface layer and volatile SO_2 [3]. A direct correlation between the surface reactions and the CL degradation is readily apparent. The Zn signal is constant depicting no change in the Zn surface concentration. This is expected as the Zn of the dissociated ZnS bonds with O^- to form ZnO.

Figure 4.2 shows the change in CL intensity and APPHs of S, C, O and Zn for the ZnS:Cu,Al,Au phosphor versus Coulomb dose during electron bombardment, at an oxygen pressure of 1×10^{-6} Torr and a current density of 2.5 mA/cm^2. The trend of the graphs in Figure 4.1 and 4.2 is the same. The Coulomb dose to get to the same amount of degradation in CL is, however, much lower in the case of the measurements at the low current density. The surface reaction rate (decrease in S APPH) is also much higher at the lower current density.

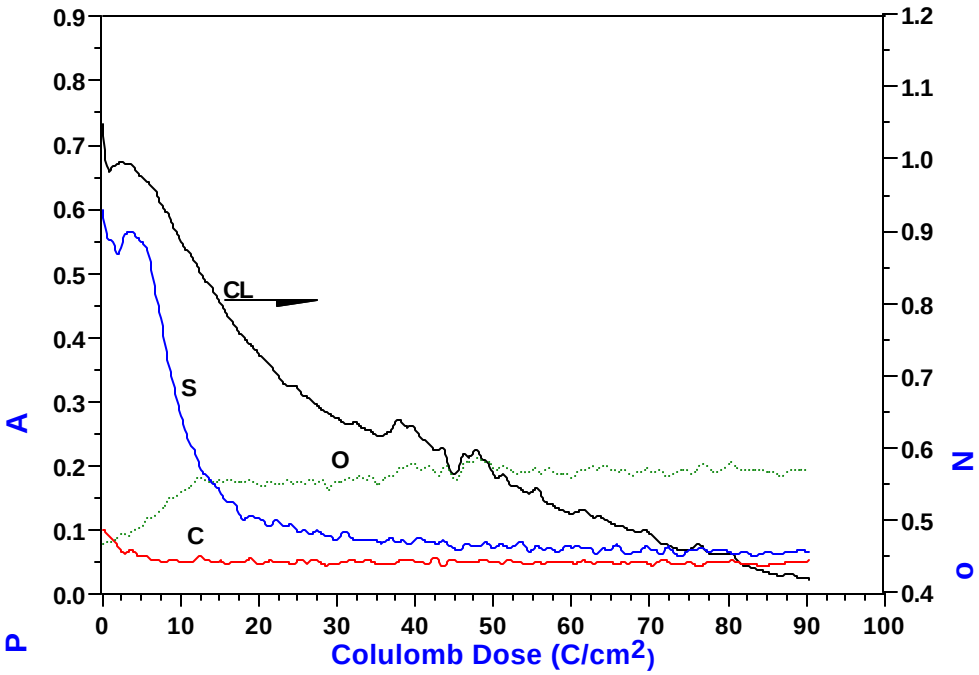

Figure 4.2 The APPHs of S, C, O and Zn as well as the CL measured at a current density of 2.5 mA cm^{-2} as a function of Coulomb dose.

A direct correlation between the changes in APPHs and the degradation in CL intensity measured at all the other electron current densities was obvious throughout this study.

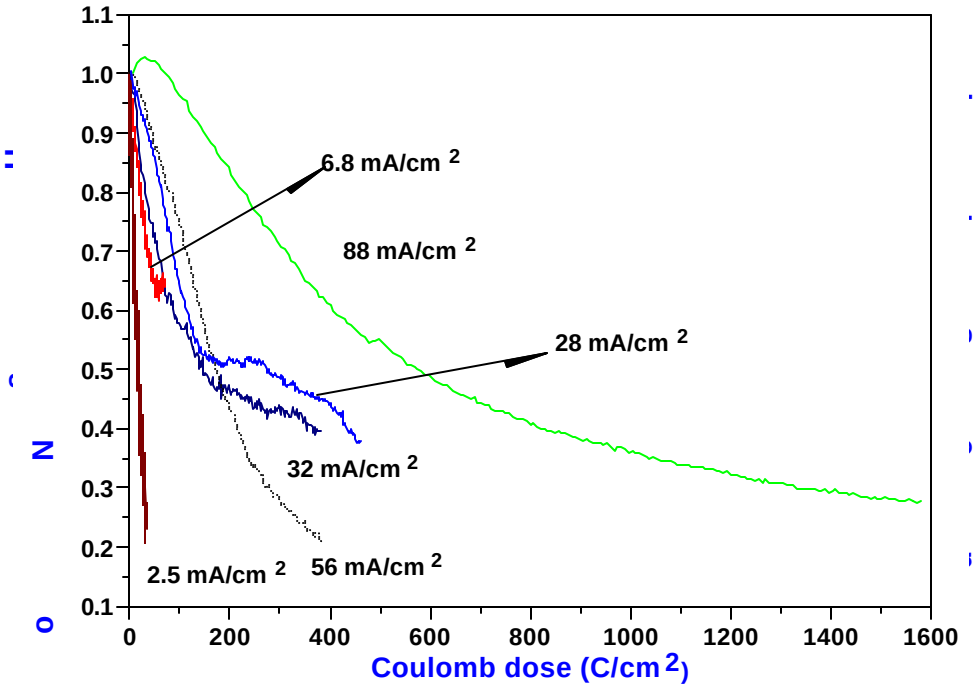

Figure 4.3 Normalised APPHs of sulphur at different electron current densities as a function of Coulomb dose.

Figure 4.3 shows the normalised APPHs of S, measured at different electron current densities, as indicated. The change in S APPHs is a direct indication of the surface reaction rate. The reaction rate at the highest electron current density (88 mA/cm^2) appears to be the lowest. While the reaction rate at the lowest electron current density is the highest, with an intermediate region where the reaction rates are more or less the same.
The mean surface lifetime of a molecule [4] is given by equation (1)

$$\tau_a = \tau_0 \exp\left(\frac{\Delta H_{des}}{kT}\right), \qquad (1)$$

where

$$\tau_0 = \frac{1}{\upsilon_o}\left(\frac{f}{f^*}\right)$$

τ_0 is a combination of the molecular partition functions of the system in the equilibrium (f), the activated states (f^*) and the vibration frequency (υ_o) of the crystal lattice. H_{des} is the desorption energy, k the Boltzmann's constant and T the temperature. A given molecule will spend a longer time near the surface at a lower temperature. One reason for the increase in the surface reaction rate at a lower current density might therefore be that at lower beam currents there is less heating due to the electron beam and therefore a higher concentration of adsorbed molecules on the surface at the lower temperature. A sample holder was constructed for cooling purposes and the above statement has been proved with more experiments at lower temperatures (see Chapter 9). It must be pointed out that the reaction depends on the dissociation of the oxygen molecule by the incident electron beam and therefore the reaction rate would not be affected exponentially through the activation energy of the reaction at such low temperature. The time the oxygen spends on the surface however would be of the outermost importance.

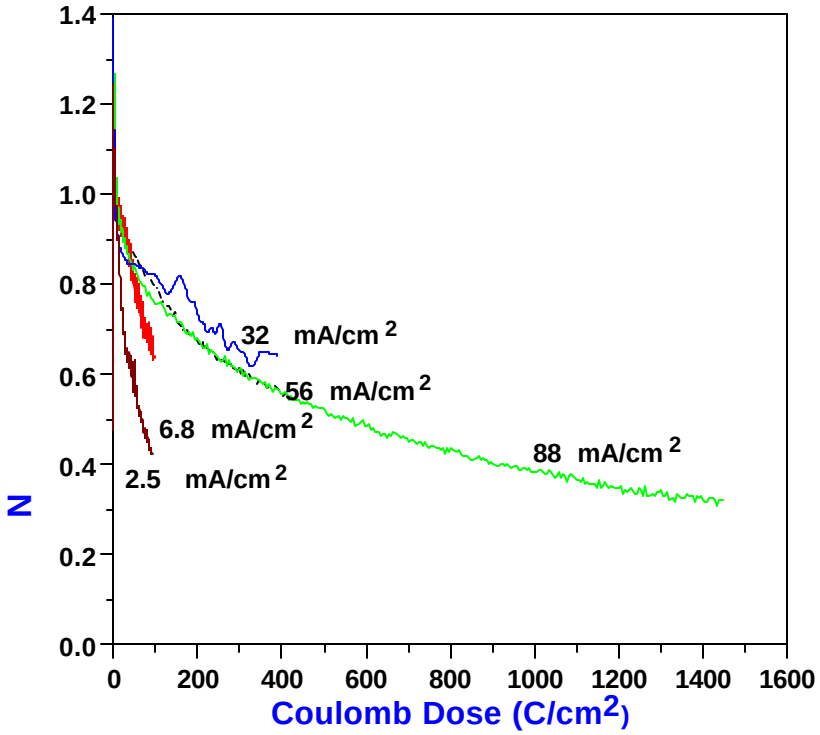

Figure 4.4 Normalised CL intensities measured at different electron current densities as a function of Coulomb dose.

The normalised CL intensities measured during electron bombardment at the different electron current densities are shown in Figure 4.4. The increase in CL degradation measured at the lower current densities is clear. The degradation at intermediate and higher current densities, however, was within experimental error the same. The electron energy position of the S peaks measured at the beginning and at the end of the experiments that were done at the different current densities showed no shift in energy for the higher current (32 mA/cm^2 and higher) densities but for the lower electron current densities a positive shift of 1 eV was measured, probably due to surface charging. When incident light falls on the surface of a photo-conductor, the photon energy may be sufficient to move valence electrons into the conduction band. Electron-hole pairs are generated in the process. The resulting increased density of charge carriers due to the light intensity makes the material more conducting. This effect is applied in light dependent resistor. The same happens if the temperature of a thermistor increases. Electrons with sufficient energy might have the same effect when falling in on a semiconductor [5,6]. Electrons are moved from the valence band into the conduction band. A lower electron

current density might therefore lead to a lower conductivity of the phosphor. In a previous [7] experiment it was proved that charging of the phosphor leads to a much more severe CL degradation, but not necessary to an increase in the surface reaction rate. The energy shift of 1 eV during electron bombardment at the lower current density is therefore attributed to the decrease in conductivity of the phosphor. The shape of the S peaks remained the same during electron bombardment. This means that S did not change the chemical environment on the surface during electron bombardment.

If the APPHs are plotted against oxidation time and not electron dose some of the data collected at higher and lower current densities followed the same trend and it took the same time to be degraded. The arrival rate of the electrons at these current densities exceeds that of the oxygen molecules by orders of magnitude. Another possibility is therefore that there is a fixed probability for an electron stimulated surface chemical reaction that only depends on adsorption or reflection of an arriving oxygen molecule as long as there are enough electrons to stimulate the reaction. This however still has to be proved in the future.

The increase in degradation of the CL and the surface reaction rate at lower electron current densities may therefore be a combination of effects. Firstly the lower temperature of the surface caused by a low current density of the electron beam may lead to an increase in the surface reaction rate due to the longer time spent by the adsorbed molecules on the surface, with a direct increase in the ESSCR probability. Secondly the lower current may lead to a lower conductivity of the phosphor which in turn leads to an increase in the CL degradation rate due to band-bending where the electron and hole (which are responsible for the light generation) are swept apart before recombination. Thirdly the reaction rate may only depend on the rate of adsorption or reflection of an arriving oxygen molecule as long as there are enough electrons to stimulate the reaction.

4.3. Conclusion

It is absolutely clear that electron beam stimulated surface reactions will occur on phosphor surfaces and will generally degrade the CL intensity and therefore degrade the phosphor efficiency. The effect of the electron current density would be critical in the overall design of the FED. The increase in temperature and charging would greatly affect the overall lifetime and performance of the FED screen. Low current densities would lead to surface charging due to a lower electron conductivity of the phosphor and to higher surface reaction rates at lower surface temperatures. The surface reaction rate also depends on the rate of adsorption or reflection of an arriving oxygen molecule.

References:

[1] H.C. Swart, T.A. Trottier, J.S. Sebastian, S.L. Jones and P.H. Holloway, J. Appl. Phys. **83** (1998) 4578.

[2] H.C. Swart, L. Oosthuizen, P.H. Holloway and G.L.P. Berning, Surf. Interface Anal., **26 (5)** (1998) 337.

[3] L. Oosthuizen, H.C.Swart, P.E. Viljoen, P.H. Holloway and G.L.P Berning, Appl. Surf. Sci., **120** (1997) 9.

[4] J.B. Hudson, *Surface Science: An Introduction*. Butterworth-Heinemann, Boston, (1992)

[5] R.G. Schulze and B.A. Kulp, J. Appl. Phys. **33** (1962) 2173.

[6] J.W. Corbett, in *Electron Radiation Damage in Semiconductor and Metals*, Academic Press, New York (1966), p 194.

[7] H.C. Swart, A.P. Greeff, P.H. Holloway and G.L.P Berning, Appl. Surf. Sci., **140** (1999) 63.

Chapter 5

The effect of temperature on the degradation of the phosphor powder in an O_2 ambient

5.1. Introduction

The influence of local heating generated by the electron beam on the degradation of the phosphors is still unknown. In the previous chapter it was concluded that lower current densities lead to higher surface reaction rates due to lower surface temperatures. The surface reaction rate also depends on the rate of adsorption or reflection of an arriving oxygen molecule, which depends on the temperature of the surface [1].

In this chapter Auger electron spectroscopy (AES) and Cathodoluminescence (CL), both excited by the same electron beam were used to monitor changes in surface composition and luminous efficiency of ZnS:Cu,Al,Au phosphor during electron bombardment at different temperatures in the presence of O_2. The changes were monitored for both sputtered and unsputtered surfaces.

5.2. AES and CL at different temperatures of the sample.

The CL intensity and APPHs (Auger Peak to Peak Heights) of S, C, O and Zn for the ZnS:Cu,Al,Au phosphor versus Coulomb dose at temperatures of 46, 200 and 300 ^oC during electron bombardment, at an oxygen pressure of 2×10^{-6} Torr, are shown in Figure 5.1(a), (b), and (c), respectively.

During electron bombardment both the C and S signals decrease exponentially for all the different temperatures. Concurrent with the decrease in C and S signals the O peak signal increased. This is due to the formation of a ZnO surface layer and volatile SO_2 [2].

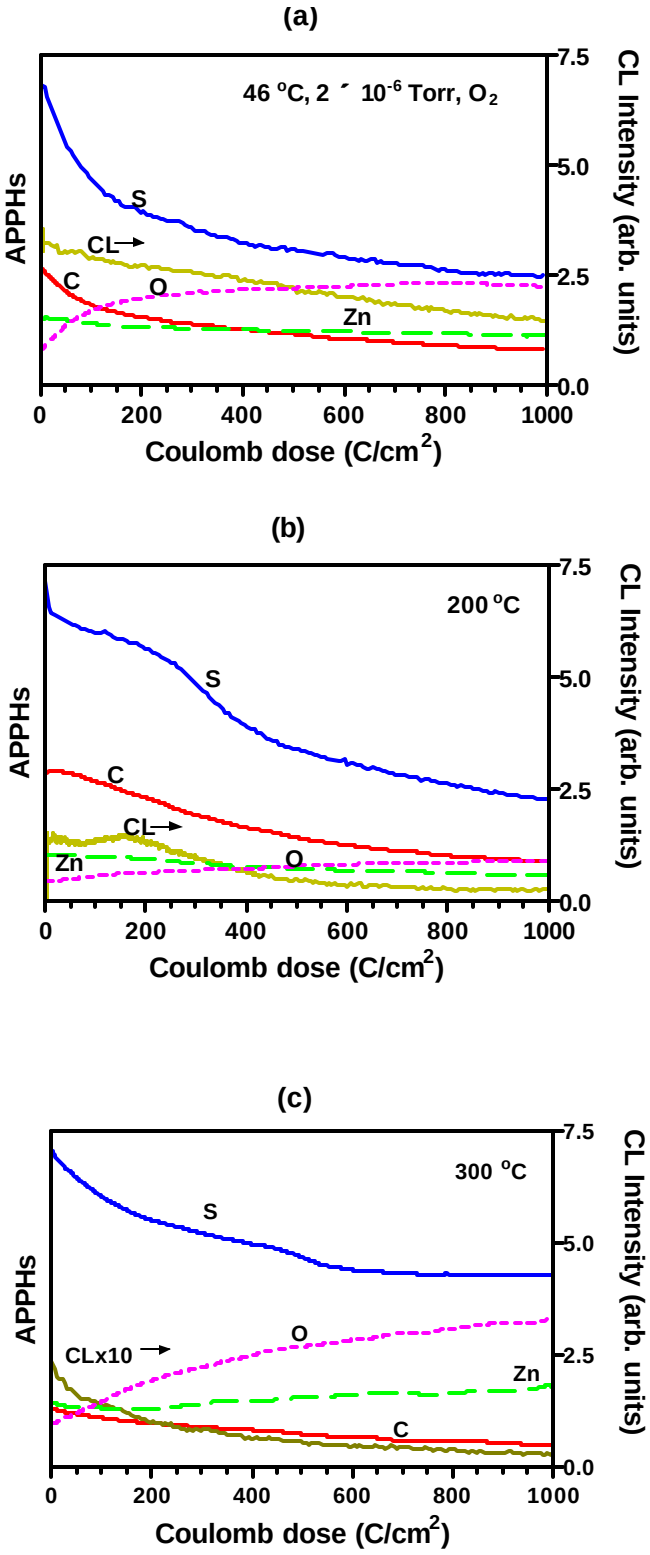

Figure 5.1 APPHs of S, C x 5, O and Zn as well as the CL as a function of Coulomb dose measured at a current density of 88 mA/cm^2 at temperatures of (a) 46 °C, (b) 200 °C and (c) 300 °C as indicated.

A direct correlation between the surface reactions and the CL degradation is readily apparent from the figures. The reaction rate, represented by the gradient of the S peak against Coulomb dose decreases at higher temperatures (see Figure 5.1(a) to (c)). Again it was clear from the experiments that the amount of C on the sample is crucial to the degradation rate. In Figure 5.1(b), the first part up to 200 C/cm^2 is dominated by adventitious carbon on the surface that varies with the degraded surface spot and the onset of degradation can only occur when the carbon is depleted from the surface [3]. In Figure 5.1 (c), the sulphur APPH against coulomb dose has a smaller gradient characteristic of the lower surface reaction rate. At higher temperatures, the mean surface stay time of O_2 at the surface decreases [1] resulting in the lower rate of dissociation of O_2 by the electron beam and thus a lower degradation rate.

It is also clear from Figure 5.1(a) to (c) that the initial CL intensity decreases with an increase in temperature. The CL intensity as function of temperature at a background pressure of 2×10^{-9} Torr before any degradation is shown in Figure 5.2.

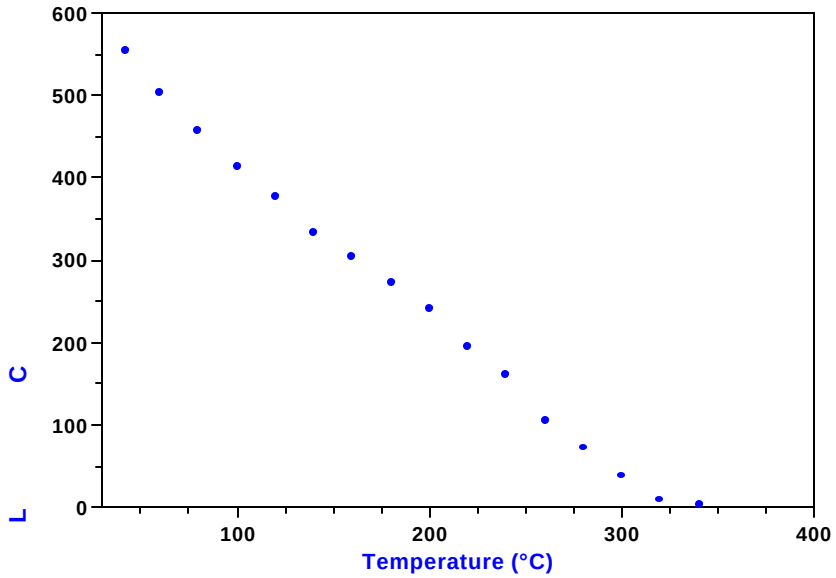

Figure 5.2 The CL intensity as function of temperature at a pressure of 2 ´ 10^{-9} Torr before any degradation.

The decrease in intensity with an increase in temperature is in accordance with thermal quenching which is explained by the configuration co-ordinate model (see sec 2.3.4 in Chapter 2). In this model the thermal vibrations of atoms surrounding the luminescent centre at high temperatures transfer the energy away from the luminescent centre resulting

in non-radiative recombination and the vibrational energy being dissipated into the host lattice as phonons. This process dominates at higher temperatures and leads to a decrease in CL intensity. On cooling down the sample, the CL intensity recovered with no deviations from the annealing trend.

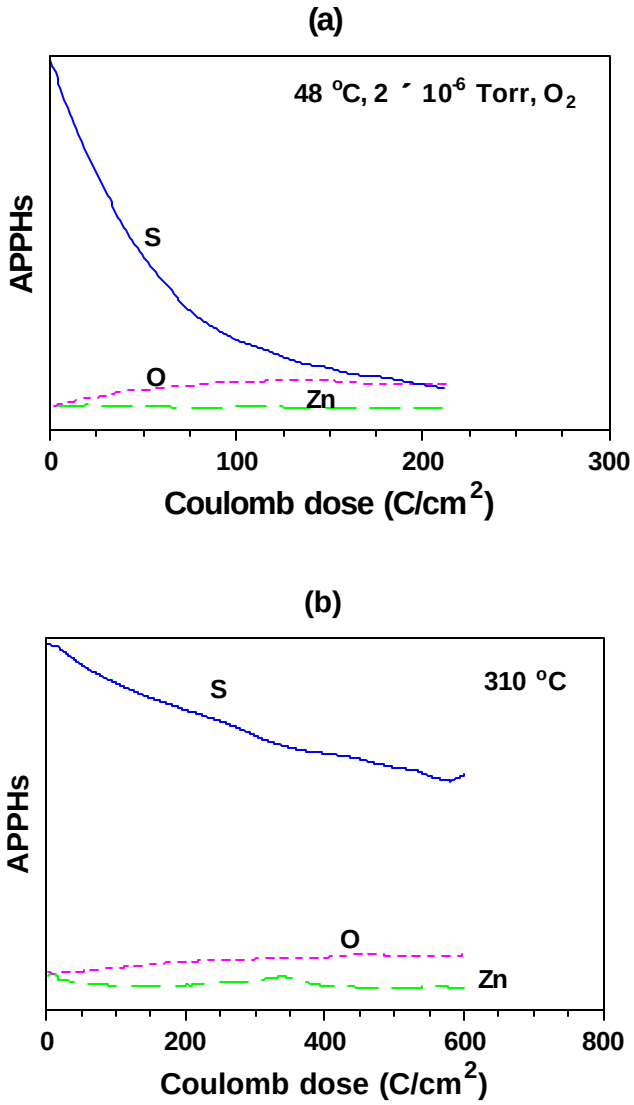

Figure 5.3 APPH of S, O and Zn as a function of Coulomb dose measured at a current density of 88 mA/cm^2 at temperatures of (a) 48 °C and (b) 310° C, as indicated, after sputtering.

Figure 5.3 (a) and (b) shows the respective APPHs of S, O and Zn for the ZnS:Cu,Al,Au phosphor versus Coulomb dose at 46 ^{o}C and 310 ^{o}C during electron bombardment, at an oxygen pressure of 2×10^{-6} Torr after sputter-cleaned with Ar^{+} ion bombardment. Figure 5.3 (c) is the change in the S APPHs as a function of Coulomb dose and time at 260 ^{o}C.

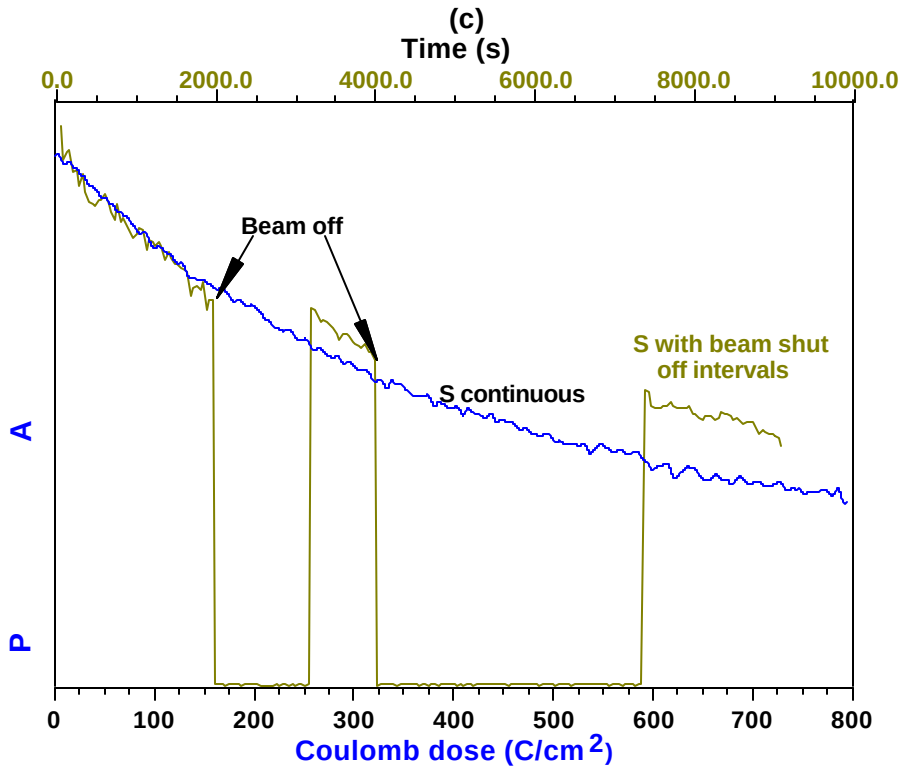

Figure 5.3 (c) APPHs of S as a function of Coulomb dose and time for continuous bombardment and with beam shut off intervals, as indicated, measured at a current density of 88 mA/cm^2 at a temperature of 260 °C, after sputtering.

The reaction on the surface was monitored at 260 ^{o}C during continuous electron bombardment (indicated by S continuous in Figure 5.3 (c)) and also when the beam was twice turned off for a few minutes during electron bombardment on a continuous oxygen exposure (indicated by S with beam shut off intervals in the Figure 5.3 (c)), with "beam off" indicating when the electron beam was switched off. The influence of the electron beam on the degradation of the ZnS surface is quite clear in Figure 5.3 (c). Each time the beam was turned off the reaction was suspended. This is a clear indication that even at higher temperatures (without the presence of the electron beam) no reaction between the oxygen and the ZnS occurred on the surface. This is in agreement with previous measurements at room temperature [3]. The trend in the profiles in Figure 5.3(a), (b) and (c) is the same. The surface reaction rate (represented by the S APPH) is, however, much higher at 46^{o}C. The Coulomb dose needed to reach 60% of the original S signal as function of temperature are shown in Figure 5.4.

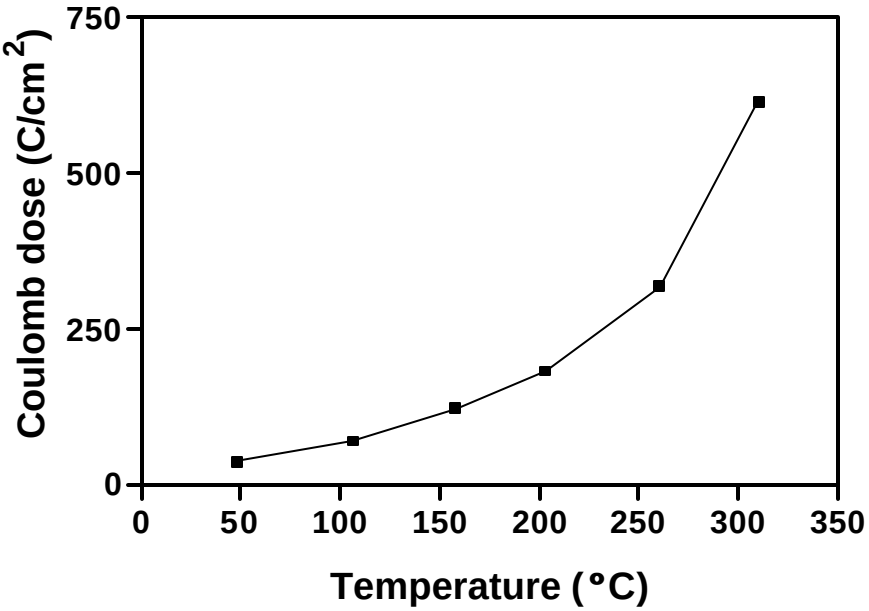

Figure 5.4 The Coulomb doses required to reach 60% of the original S signal as function of temperature

The Coulomb dose for the ZnS sulphur APPH to reach 60% of the original intensity increases exponentially with an increase in temperature. This indicates that the surface reaction rate decreases exponentially with an increase in temperature from room temperature up to 310 ^{o}C, which is in agreement with the thermodynamic and kinetic view of a gas/surface interface.

In the following section, some of the expressions were stated, discussed and cited in Chapter 2 under the section on the mathematical interpretation of the degradation model, but will also be stated herein after for undistracted reading. This section substantiates the above conclusion that the surface reaction rate decreases with an increase in temperature when all the variables are kept constant except the temperature, at this specific temperature range (45°C to 300 °).

For the substrate atom undergoing a reaction followed by desorption, the rate of change of the surface concentration, C_s can be expressed as [4]

$$\frac{dC_s}{dt} = -k' C_{as} C_s, \tag{1}$$

where k' is a chemical rate constant which depends on the activation energy of the chemical reaction and C_{as} is the concentration of the adsorbed atomic species that will react with the ZnS. The value of k' typically increases exponentially with an increase in temperature. The concentration of the adsorbed atomic specie is:

$$C_{as} = N \sigma_{ma} n_a J \tau_{as} \tag{2}$$

where N is the number of reactive atomic species produced from the parent molecule and depends upon the composition of the gases, σ_{ma} is the dissociation cross section of the molecules to atoms (which is a function of electron energy and current density [5]), n_a the surface population of the adsorbed molecules per square centimetre, J is the electron flux density (electrons $cm^{-2}s^{-1}$), and τ_{as} is the lifetime of a reactive atomic specie. It is assumed that the rate of production of adsorbed atomic species limit the ESSCR reaction rate.

The surface population (n_a) of the adsorbed molecules per square centimetre can be expressed as

$$n_a = \sigma I \tau_a \tag{3}$$

where σ is the sticking coefficient, I the molecular impingement rate and τ_a the mean surface lifetime of a molecule. Substituting expressions for I and τ_a into equation 3 leads to

$$n_a = \sigma \left(\frac{P}{(2\pi m k T)^{1/2}} \right) \left(\tau_0 \exp\left(\frac{\Delta H_{des}}{kT} \right) \right) \tag{4}$$

where P is the pressure, m the molecular mass, T the temperature, k Boltzmann's constant, τ_0 is a combination of the molecular partition functions of the system in the equilibrium and activated states and the vibration frequency of the crystal lattice, and H_{des} is the desorption energy.

Substituting equations (2 and 4) into (1) leads to

$$\frac{dC_s}{dt} = -k'C_s N f_{ma} J t_{as} s\left(\frac{P}{(2\pi mkT)^{1/2}}\right)\left(t_0 \exp\left(\frac{\Delta H_{des}}{kT}\right)\right) \qquad (5).$$

In these experiments all the parameters were kept constant except the temperature. The dependence of the surface reaction upon T would be determined by the magnitude of the positive desorption energy (ΔH_{des}) of the physisorption process versus the negative activation energy in the chemical rate constant (k'). The $T^{-1/2}$ results from the impingement rate of gas from the vacuum and is controlled by the temperature of the vacuum system walls and can typically be ignored relative to the exponential dependence of the third term in equation (5). The experimental results obtained here (Figure 5.4) indicate clearly that the surface reaction rate decreases exponentially with an increase in temperature from room temperature to 310 ^{o}C. The reaction rate at this temperature range (46 ^{o}C to 310 ^{o}C) is therefore controlled by this term that is the mean surface lifetime of the absorbed molecule.

Thermodynamically it is possible to form ZnO from ZnS in the presence of oxygen. Possible reactions are:

$$ZnS + 2O_2 \leftrightarrow ZnO + SO_3(g) \qquad (A)$$

$$2ZnS + 3O_2 \leftrightarrow 2ZnO + 2SO_2(g) \qquad (B)$$

Free energies of formation calculations showed that the reaction must occur at elevated temperatures. For the first reaction (A) the temperature must be in the order of 2938 °C and for the second reaction (B) the temperature must be in the order of 5701 °C (see calculations on the appendix, p 88). The entalphy and entropy values used in the calculations were from the CRC Handbook of Chemistry and Physics [6].

5.3. Conclusion

It is clear that the reaction between oxygen and the ZnS phosphor are due to electron beam stimulated surface reactions and not due to local heating of the surface by the electron

beam. The surface reaction rate depends on the dissociation cross section of the oxygen molecule and the time that an arriving oxygen molecule spends on the surface. The mean surface stay time is a function of surface temperature and decreases at higher temperatures.

References:

[1] J.B. Hudson, *Surface Science: An Introduction*. Butterworth-Heinemann, Boston, (1992)

[2] L. Oosthuizen, H.C.Swart, P.E. Viljoen, P.H. Holloway and G.L.P Berning, Appl. Surf. Sci., **120** (1997) 9.

[3] H.C. Swart, J.S. Sebastian, T.A. Trottier, S.L. Jones and P.H. Holloway, J. Vac. Sci. Technol. **A14**, (1996) 1697.

[4] Y. Darici, P.H. Holloway, J. Sebastian, T. Trottier, S Jones and J Rodriquez, J. Vac. Sci. Technol. A, **17(3)** (1999) 692.

[5] H.C. Swart, L. Oosthuizen, P.H. Holloway and G.L.P. Berning, Surf. Interface Anal., **26** (5) (1998) 337.

[6] R.C. Weast and M.J. Astle, CRC Handbook of Chemistry and Physics (CRC Press, Boca Raton, FL, 1982)

Chapter 6

Characterisation of ZnS thin films grown on Si (100) by XeCl pulsed laser ablation

6.1. Introduction

There is an augmented preference in the fabrication of activated thin film ZnS materials for phosphor screens to powder screens. Thin film phosphor materials have some advantages over powders in the FED environment. These being the reduction of light scattering and the good thermal contact between the screen and the face plate [1]. Thin luminescent films also pose no outgassing problems, possess uniform properties across the covered area and higher resolution and contrast with less material [2]. The volume occupied by the powder screen inside the FED also limits the reduction of the overall size of the devise compared to thin film screens. Several techniques on growing ZnS thin films have been reported, which include chemical vapour deposition (CVD) [3], molecular-beam epitaxy (MBE) [4], atomic layer epitaxy (ALE) [5], metalorganic chemical vapour deposition (MOCVD) [6], successive ionic layer adsorption and reaction method (SILAR) [7] and metalorganic vapour-phase epitaxy (MOVPE) [8] all of which will not be discussed in this study.

The laser deposition technique has advantages over other deposition methods because it is a pure physical mechanism without the incorporation of carbon and that the stoichiometry of the target material is maintained in the deposited films [9]. It was shown [10] that during deposition of metallic film in UHV the high kinetic energy of the ablated ions leads to re-sputtering of already deposited material. Deposition in an inert gas changes the kinetic energy distribution of the ablated particles and significantly reduces the re-sputtering of the deposited material. Increasing the target to substrate distance when depositing in vacuum could rectify the energetic plume damaging effect. Best films can be achieved by the optimisation of background pressure with the target to substrate

distance [11]. The group VI element vacancy problem may also be solved by the PLD growth method [12,13]. McLaghlin *et al.* [14] observed that 1 µm thick rf sputtered samples show weaker CL than the similar thickness of a pulsed laser deposited film.

Pulsed laser deposition (PLD) of semiconductor thin films was first reported in 1965, at the end of 1992 more than 128 different materials could be grown by PLD [15,16]. It has since developed as a materials research tool, currently being used to deposit a variety of multicomponent electronic ceramic thin films for the development of next generation electronic devices [17]. Other drawbacks of PLD are poor film uniformity and surface particles. Efforts to reduce the particulate have been reported [18] and techniques to deposit uniform films on large area (15 x 15) cm^2 have been achieved by Geer *et al.* [19].
In this chapter, the crystal structure and surface roughness of ablated ZnS phosphors on Si(100) were investigated by comparing four samples of ZnS thin films that were deposited with and without the inert gas in the deposition chamber. AES, XRD, RBS and AFM were utilised for the characterisation of the thin films.

6.2. Characterisation

Figure 6.1 shows the RBS spectrum of the ZnS:Cu,Au,Al film deposited on the Si(100) substrate.

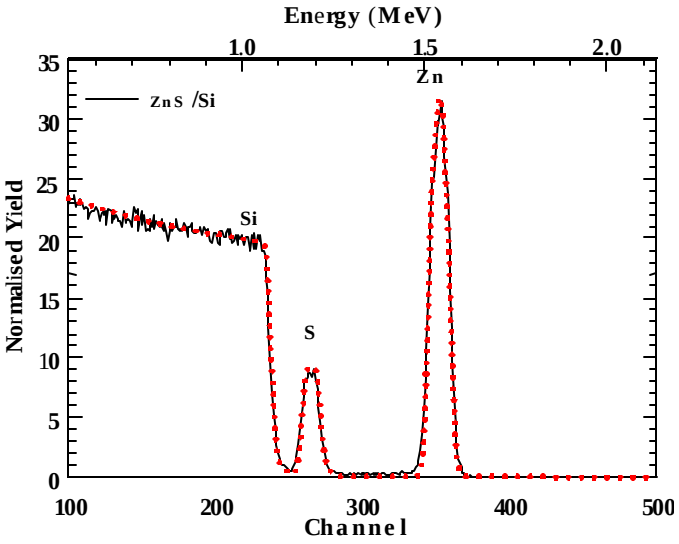

Figure 6.1 RBS spectrum of pulsed laser deposited ZnS phosphor film on Si(100), the dotted line is the ZnS 1:1 compositional simulation.

The thickness of the film was measured to be 92 nm and the simulation using the XRump program [20] indicated that ZnS was deposited. The doping elements are utilised for the specific light frequency emission and their concentration is not significant in the bulk composition.

For growth characterisation, sample 1 and 2 were prepared using 3000 laser pulses each, at a base pressure of 10^{-5} Torr. Sample 3 was deposited using 6000 laser pulses at a nitrogen gas pressure of 10^{-3} Torr and sample 4 by using 3000 laser pulses at a nitrogen pressure of 10^{-3} Torr. Figure 6.1 (a) shows the AES differential energy spectrum of sample 1 revealing the chemical composition of the surfaces before sputtering.

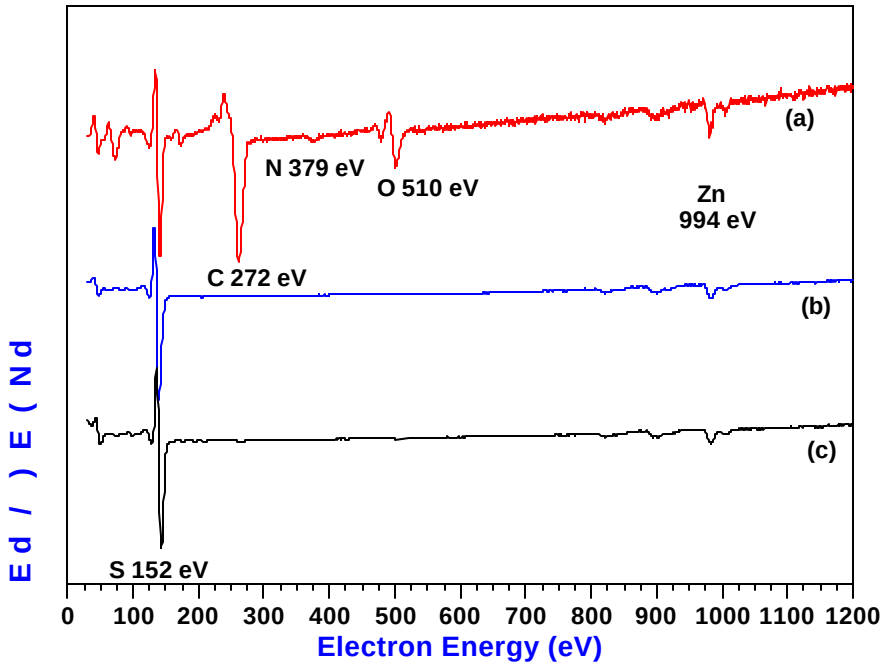

Figure 6.2 AES differential energy spectra of (a) first layer before sputtering, (b) sample 1 and (c) sample 4, both during sputtering.

Figure 6.2 (b) and (c) are the respective AES spectra of sample 1 and sample 4 acquired during sputtering which depicts uncontaminated ZnS films into the bulk. The AES spectrums for the remaining two samples had the same trend. Figure 6.3 illustrates the depth profiles of (a) sample 1 and (b) sample 4, without and with nitrogen ambient during deposition, respectively.

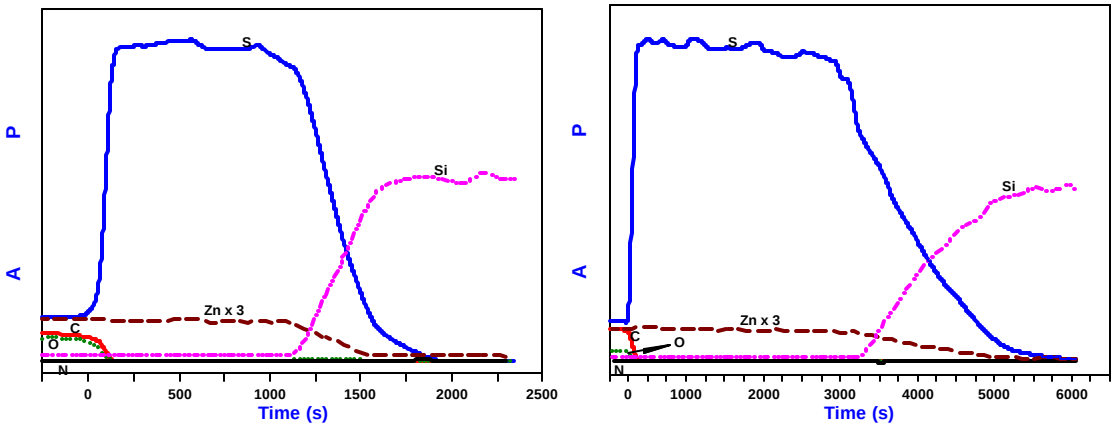

(a) **(b)**

Figure 6.3 AES depth profiles of (a) sample 1 and (b) sample 4.

The difference in the sputtering time after the adventitious carbon and oxygen are depleted on the surface is due to the different film thickness. There is no evidence of nitrogen incorporation on the surface and in the bulk of sample 4, which was grown in the nitrogen ambient.

Figure 6.4 presents (3µm x 3µm) three-dimensional renditions of the AFM images acquired on sample 1 and 4. These films were deposited using 3000 laser pulses each with the variance in the ambient pressure during deposition

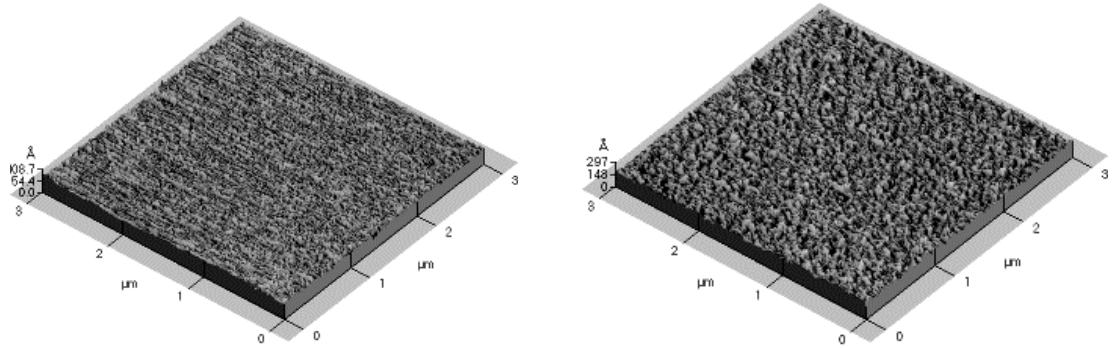

(a) **(b)**

Figure 6.4 Three-dimensional AFM images of the ZnS films deposited on Si (100), (a) Sample 1 and (b) Sample 4.

The Z scale on the images, which illustrates the height of the protruding surface features, is more extended in sample 4. The R_{rms} value depends on the heights of these surface features.

Figure 6.5 shows the statistical presentation of R_{rms} values calculated from a representative selection of captured images.

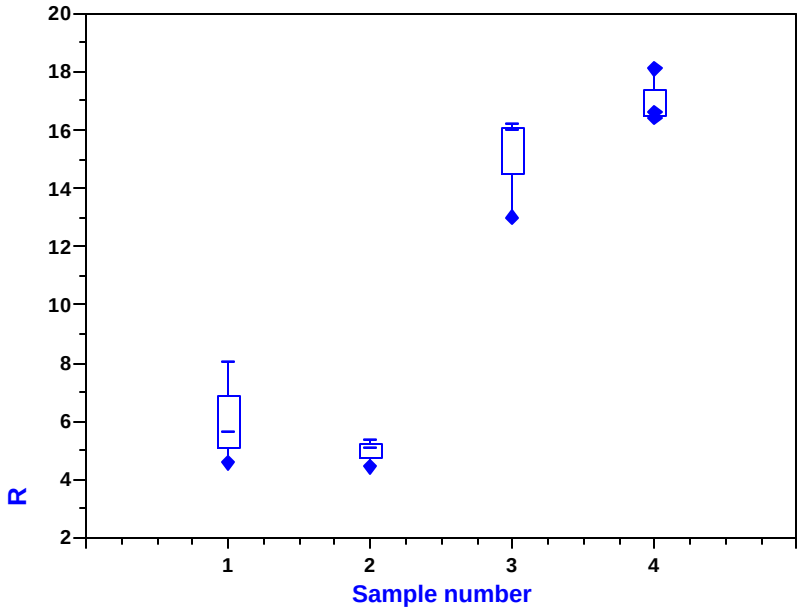

Figure 6.5 The statistical presentation of calculated rms roughness (R_{rms}) values for all the films.

These values manifest the evolution of a rougher surface with the introduction of the nitrogen gas into the deposition chamber. The increase in roughness is directly related to the plasma plume dynamics. The atoms and ions in the plasma plume collide with the background N_2 gas and their energies are reduced. Without the background pressure to slow down the plume and decrease its energy, the energetic plume partially erodes the newly formed layers resulting in a slow growth rate and a smoother surface finish. Increasing the background pressure can reduce this effect [21]. The rougher surfaces, however, would not be ideal for the operation of the FED as they would increase the scattering of light by the phosphor.

Figure 6.6 shows the RBS results of the thickness values of the films.

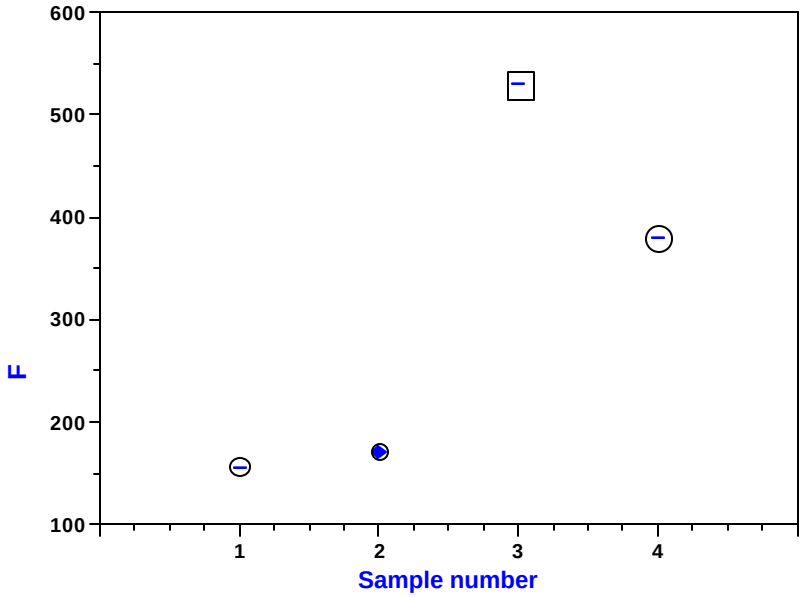

Figure 6.6 Film thickness values from the RBS measurements.

Sample 1 and 2 have approximately the same thickness, verifying the reproducibility of the experiments. There is an increase in film thickness with the introduction of N_2 gas as the slower and less energetic plasma plume is less damaging to the recently deposited films, thereby increasing the growth rate. It is also obvious that the thickness (sample 3) increases with the number of laser pulses.

Figure 6.7 shows the XRD spectrums of the thin films as well as the spectrum of target material. There is an emanation of the (100) peak on all the films, which is not well pronounced in the target material. This preferential growth is due to the influence of the Si (100) substrate that is favoured by the high mobility of the ablated species. The substrate influence on the crystalline phases of II-VI compound semiconductors grown by PLD was also observed by Shen *et al.* [11]. The increased intensity of the (100) peak in sample 4 in the presence of the N_2 gas proves the influence of the background pressure on the modification of the ablated plume for improved surface orientation.

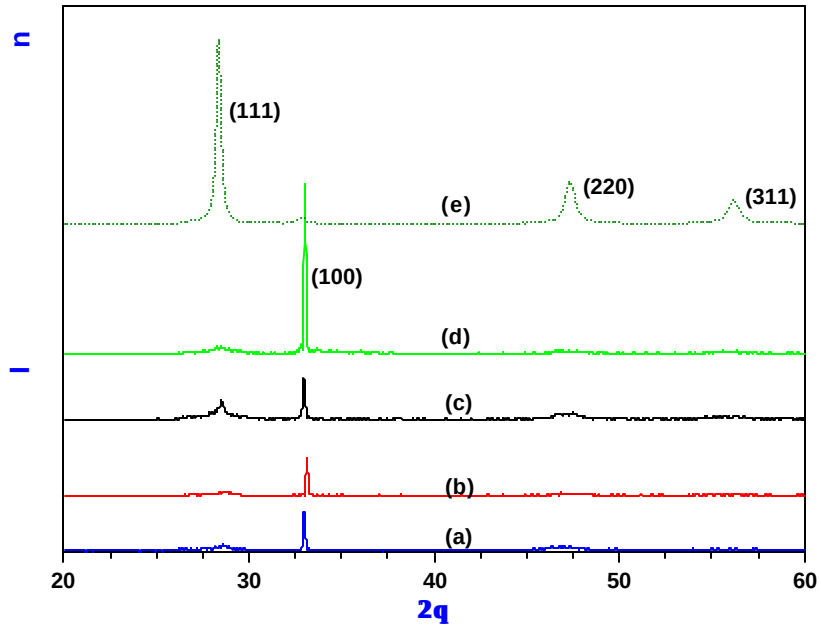

Figure 6.7 XRD spectra of the films, (a) sample 1, (b) sample 2, (c) sample 3, (d) sample 4 and (e) spectrum of the target material.

The preferential orientation that is influenced by the Si (100) substrate is more dominant in this film. Sample 3 deposited by 6000 laser pulses shows the emergence of the (111) ZnS peak. This depicts a decreasing substrate influence following an increase in the film thickness.

6.3. Conclusion

The background pressure in the deposition chamber affects the surface morphology and the orientation of the film by modifying the plasma plume as demonstrated by the high R_{rms} value of the film surface and high intensity of the (100) peak on sample 4, a sample that was deposited in a N_2 atmosphere of 10^{-3} Torr. It is also evident that the film orientation is more influenced by the substrate orientation for thinner films and this effect decreases as the deposited film thickness increases.

References:

[1] T. Hase, T. Kano, E. Nakazawa and H. Yamamoto, Adv. Electron. Electron Phys, **79** (1990) 271.

[2] G.A. Hirata, J. McKittric, M. Avalos-Borja, J.M. Siqueiros and D. Devlin, Appl. Surf. Sci. **113/114** (1997) 509.

[3] B. Greengerg, W.K. Zwicker and I. Cadoff, Thin Solid Films, **141** (1986) 89.

[4] J. W. Cook, Jr., D.B. Eason, R.P. Vaudo and J.F. Schetzina, J. Vac. Sci. Technol. **B 10(2)** (1992) 901.

[5] J. Ihanus, M. Ritala, M. Leskeläand T. Prohaska, R. Resch, G. Friedbacher and M. Grasserbauer, Appl. Surf. Sci. **120** (1997) 43.

[6] C.W. Wang, T.J. Sheu, Y.K. Su and M, Yokoyama, Appl. Surf. Sci. **113/114** (1997) 709.

[7] M. P. Valkonen, S. Lindroos, R. Resch, M. Leskelä, G. Friedbacher and M. Grasserbauer, Appl. Surf. Sci. **136** (1998) 131.

[8] P. Prete, N. Lovergine, M. Masser, C. Zanotti-Fregonora and A.M. Mancini, J. Crystal Growth, **204** (1999) 29.

[9] A. Gupta, in *Pulsed Laser Deposition of Thin Films* edited by D.B. Chrisey and G.K. Hubler (Wiley, New York, 1994), p. 265.

[10] K. Strum, S. Fähler and HU Krebs, Appl. Surf. Sci. **154-155** (2000) 462.

[11] W.P. Shen and H.S. Kwok, Appl. Phys. Lett. **65 (17)** (1994) 2162.

[12] S.D. Setzer, M. Moldovan, Zhonghai Yu, T.H. Myers, N.C. Giles and L.E. Halliburton, Appl. Phys. Lett. **70 (17)** (1997) 2274.

[13] J.T. Cheung and J. Madden, J. Vac. Sci. Technol. **B. 5 (3)** (1987) 705.

[14] M. McLaughlin, H.F. Sakeek, P. Maguire, W.G. Graham, J. Molloy, T. Morrow, S. Laverty and J. Anderson, Appl. Phys. Lett., **63 (14)** (1993) 1865.

[15] J.T. Cheung, in *Pulsed laser deposition of thin films,* edited by D.B. Chrisey and G.K. Hubler (Wiley, New York, 1994), p 1.

[16] K.L. Seanger, in *Pulsed laser deposition of thin films,* edited by D.B. Chrisey and G.K. Hubler (Wiley, New York, 1994), p 581.

[17] J.S. Horwitz, D.B. Chrisey, R.M. Stroud, A.C. Carter, J. Kim, W. Chang, J.M. Pond, S.W. Kirchoefer, M.S. Osofsky and D. Koller, Appl. Surf. Sci. **127-129**, 507, 1998.

[18] P.K. Schenck, M.D. Vaudin, D.W. Bonnell, J.W. Hastie and A.J. Paul, Appl. Surf. Sci. **127-129** (1998) 655.

[19] J.A. Geer and M.D. Tabat, J. Vac. Sci. Technol. **A 13(3)** (1995) 1175.

[20] www.genplot.com

[21] D.B. Geohegan, in *Pulsed Laser Deposition of Thin Films* edited by D.B. Chrisey and G.K. Hubler (Wiley, Ney York, 1994), p. 115.

Chapter 7

Electron beam induced degradation of a pulsed laser deposited ZnS:Cu,Au,Al thin film on a Si(100) substrate

7.1. Introduction

There are still some drawbacks inherent to the thin film screens. The light output of the films is much less than light generated by the phosphor powders. This is probably due to the large surface area of the powdered material exposed to the addressing electron beam. Jones *et al.* [1], showed that the efficiency response of the Eu:Y_2O_3 phosphor films that were laser deposited was about 10% relative to that of the target powder. Although uniform screens up to 15 x 15 cm^2 have been fabricated using by pulsed laser deposition technique [2], there are still some technical constraints to the deposition of uniform films exceeding these dimensions to be utilised for big display purposes.

In this chapter, the degradation of ZnS:Cu,Au,Al thin phosphor film in 5 x 10^{-7} Torr of O_2 and CO_2 ambient and at different electron beam energies, is investigated. Although the CO_2 is one of the residual gases in a vacuum, it was also anticipated that C from the dissociation of CO_2 would be deposited on the surface of the phosphor film therefore hindering the onset of degradation. AES and CL both excited by the same electron beam have been utilised to monitor the changes in surface and the CL efficiency of the thin film during electron bombardment.

7.2. AES and CL analysis

The thickness of the film measured by RBS was 530 nm and it had a continuous coverage over the entire surface (from the AFM images) on page 56. Figure 7.1 shows the AES spectra of (a) the film before degradation and, (b) and (c), after degradation by a Coulomb dose of about 300 C/cm^2 in O_2 and CO_2 ambients, respectively. The AES spectrum before

degradation exhibits the peaks of adventitious C and a pronounced sulphur peak on the surface of the phosphor.

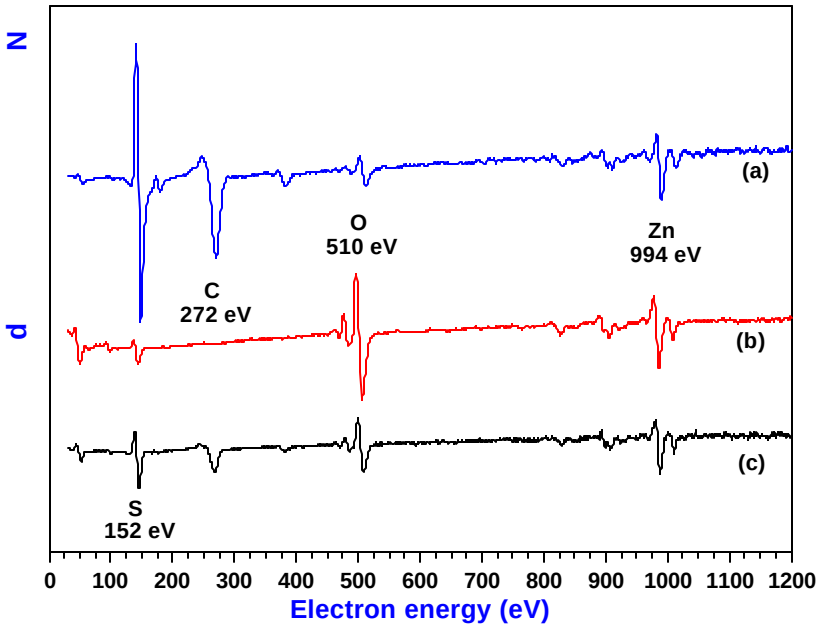

Figure 7.1 AES differential energy spectra of (a) film before degradation, (b) and (c) film after degradation for a Coulomb dose of about 300 C/cm^2 in O_2 and CO_2, respectively.

The spectrum acquired after degradation in O_2 ambient displays a surface depleted of C. There is C left on the surface after degradation in the CO_2 environment that was introduced from dissociation of CO_2, but the peak intensity drastically decreases during the electron degradation process. There is less S and more O in (b) in contrast to a relative higher concentration of S and less O shown in (c) after the same Coulomb dose.

Figures 7.2 (a) and (b) show the Auger peak to peak heights (APPH) of the elements on the surface of the phosphor and the CL measured against Coulomb dose during degradation in an O_2 and CO_2 gas environment, respectively. They both illustrate the ESSCR mechanism in which the S and C are reduced and O increases on the surface. The increase in O is due to the formation of ZnO on the surface. The reduction of S and C are due to desorption by formation of volatile SO_2 and CO_x [3]. The profile showing the diminishing of S APPH with Coulomb dose also depicts the rate of electron stimulated

chemical reaction on the surface. The CL intensity in Figure 7.2 (a) decreases more severely compared to the CL intensity in Figure 7.2 (b).

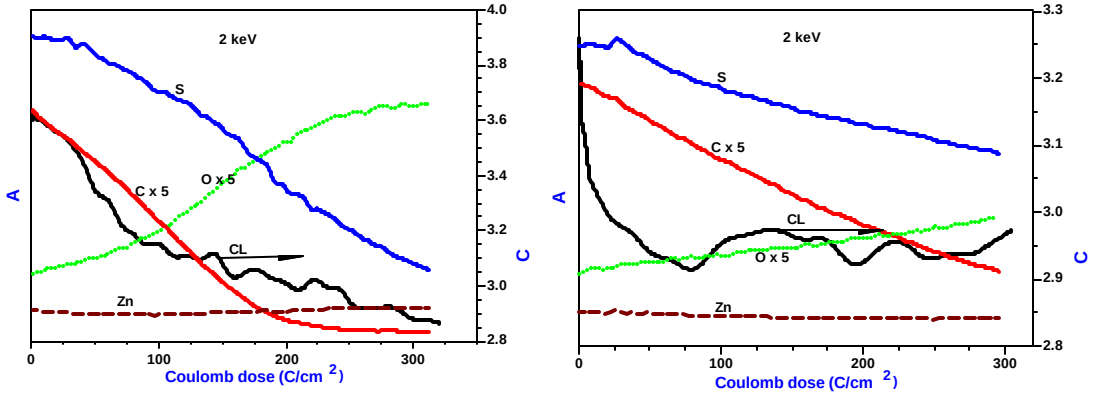

(a) **(b)**

Figure 7.2 The APPH of S, C, O, and Zn as well as the CL measured during degradation in a 5 x 10^{-7} Torr O_2 ambient (a) and a 5 x 10^{-7} Torr CO_2 ambient (b) as a function of Coulomb dose.

This is attributed to the amount of C that is on the surface during electron bombardment, which is coming from CO_2 and it prevents oxidation.

The chemical reaction likely to occur in the O_2 environment is as follow:

$$2ZnS + 3O_2 \Leftrightarrow 2ZnO + 2SO_2 \quad (1)$$

Calculating the energy of formation, ΔH.

$2(-46.04) + 3(0) \Leftrightarrow 2(-83.24) + 2(-70.94)$

$\Delta H = -72.09$ kcal/mol O_2.

The above equation has a negative energy of formation and was proved to occur during electron bombardment of ZnS in O_2 by Oosthuizen *et al.* [3]. The numbers in brackets are the free energies of formation of the reactants and products during the formation of ZnO.

There are probably two reactions that compete during electron bombardment in CO_2 partial pressures. Darici *et al.* [4], proposed a reaction in which the elemental C is deposited on the surface during degradation, equation (2)

$$ZnS + 3/2CO_2 \Leftrightarrow ZnO + 3/2C + SO_2 \quad (2)$$

Calculating the ΔH yields,

$(-46.04) + 3/2(0) \Leftrightarrow (-83.24) + 3/2(0.4533) + (-70.94)$

$\Delta H = -71.64$ kcal/mol CO_2.

Equation 2 is thermodynamically possible and the results (AES spectrum Figure 7.1 (c)) confirm that there is still some carbon on the surface of the phosphor after electron bombardment in CO_2, compared to Figure 1(b) in the O_2 ambient after the same Coulomb dose of about 300 C/cm^2. However, Figure 7.2 (b) also shows that the C APPH is declining with Coulomb dose although not to the extent similar to the O_2 ambient during electron bombardment. These observations lead to a proposal of another reaction that competes with the above reaction, equation (3)

$$ZnS + 3CO_2 \Leftrightarrow ZnO + 3CO + SO_2 \qquad (3)$$

Calculating the ΔH gives

$(-46.04) + 3(0) \Leftrightarrow (-83.24) + 3(-26.416) + (-70.94)$

$\Delta H = -62.44$ kcal/mol CO_2

The ΔH of the above is negative which implies that the reaction is thermodynamically possible. In equation (3) another species, CO, is released into the vacuum. These two reactions (equations 2 and 3) are probably competing during electron bombardment in the CO_2 ambient, hence the slow rate of both the formation of ZnO in the surface (shown by the slow increase of O coverage, Figure 7.2 (b)) and desorption of S as C is also deposited on the surface of the phosphor (equation 2). The above explanation agrees with the ionisation and dissociation mechanisms of CO_2 upon electron beam impact of Tian and Vidal [5]. Their experiments showed that the most likely primary incident is single ionisation of CO_2 to CO_2^+ as the cross section of single, double and triple ionisation decreases by at least one order of magnitude as the ionisation degree increases by 1. The ionisation is followed by the dissociation of CO_2^+ with one of the dissociation channels being,

$$CO_2^+ \rightarrow O^+ + (C, O). \qquad (4)$$

The symbol (C, O) means that the products can either be two separate atoms C and O or a CO molecule. It has been further confirmed that, at high electron energies, this dissociation channel has the highest cross-section among other dissociation channels [6]. The above statements substantiate the fact that C can be deposited on the surface and that CO can be released into the vacuum through the electron beam impact with CO_2 adsorbed on the surface. The peak shapes from the Auger spectra reveal that C was in the graphite form throughout the electron bombardment.

Figure 7.3 shows the normalised sulphur APPH plotted against Coulomb dose for 2, 3 and 4 keV during degradation in a 5 x 10^{-7} Torr O_2 ambient. As the energy of the electron beam is increased the S APPH decline slows. The electron impact ionisation cross section for an atom decreases with an increase in primary electron energy at higher energies (> 2 keV) [7].

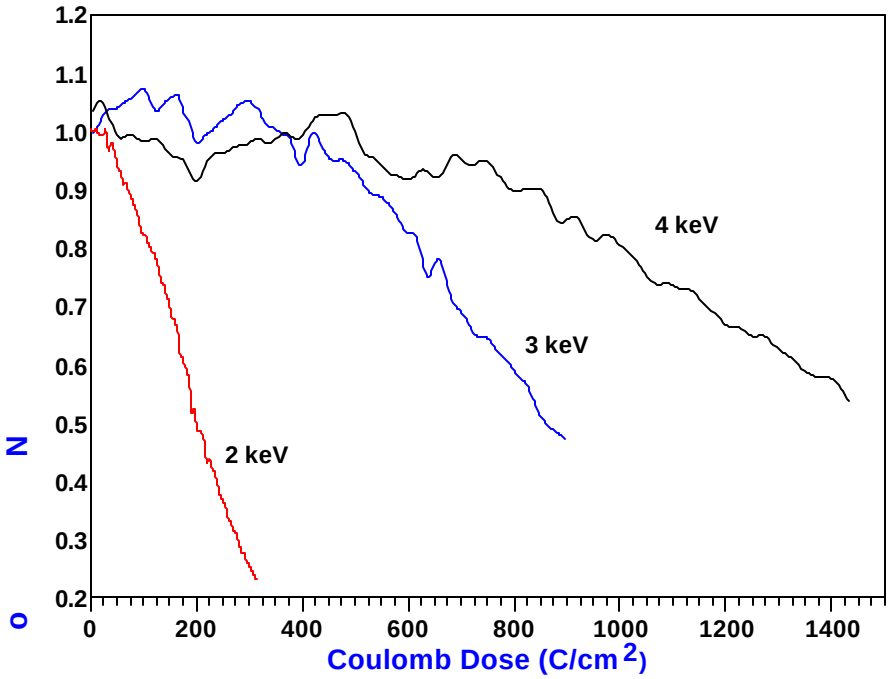

Figure 7.3 Normalised APPH of sulphur for different electron beam energies as a function of Coulomb dose at an O_2 pressure of 5 x10^{-7} Torr.

The rate at which the S and O atoms are ionised during the surface reactions will therefore decrease with an increase in electron energy. This will lead to a decrease in the desorption of S and the formation of ZnO layer on the surface with increasing primary electron beam energy, as seen in Figure 7.3. The same trend was observed for the ZnS phosphor powders [8].

The CL brightness plotted against the primary electron beam energy is shown in Figure 7.4. The CL brightness increases exponentially with the increasing primary electron beam energy. This is consistent with the increase in the excitation of the free carriers at higher beam energies, which subsequently recombine and is detected as CL. The volume over which minority carriers are generated by an electron beam, increases with the increasing

electron beam energy [9]. The experimental results obtained here indicate clearly that the degradation rate decreases with an increase in primary electron energy and also that the CL intensity increased with an increase in primary electron energy.

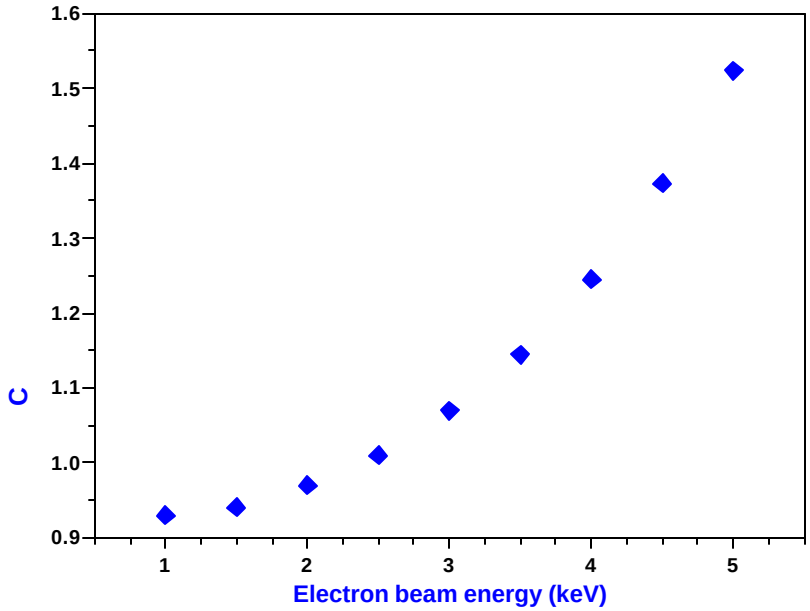

Figure 7.4 CL intensity at different electron beam energies.

The problem, however, is that a phosphor is needed to perform well at the lower voltages to be used in the FED environment.

7.3. Conclusion

ZnS:Cu,Au,Al thin films deposited by pulsed laser degraded according to the ESSCR mechanism. The comparison between O_2 and CO_2 as ambient gasses during electron bombardment reveals that the phosphor screen will degrade faster in a vacuum with a higher O_2 partial pressure than CO_2. There are two competing reactions that might occur in the CO_2 ambient, which reduced the rate of degradation of the thin film. The rate of electron stimulated chemical reactions on the surface in O_2 ambient were limited by the energy of the primary electron beam. This is due to the ionisation cross section profile for an atom, which decreases with an increase in the primary electron energy at higher energies (> 2kV). The luminous intensity of the film increased with the primary electron beam energy.

References:

[1] S.L. Jones, D. Kumar, R.K. Singh and P.H. Holloway, Appl. Phys. Lett., **71 (3)** (1997) 404.

[2] J.A. Geer and M.D. Tabat, J. Vac. Sci. Technol., **B 5(3)** (1998) 1175.

[3] L. Oosthuizen, H.C. Swart, P.E. Viljoen, P.H. Holloway and G.L.P. Berning, Appl. Surf. Sci., **120** (1997) 9.

[4] Y. Darici, P.H. Holloway, J.S. Sebastian, T.A. Trottier, S.L. Jones and J. Rodriquez, J. Vac. Sci. Technol., **A 17(3)** (1999) 692.

[5] C. Tian and C.R. Vidal, J. Chem. Phys., **108(3)** (1998) 927.

[6] C. Tian and C.R. Vidal, Phys. Rev., **A 58** (1998) 3783.

[7] L.E. Davis, N.C. MacDonald, P. W. Palmberg, G.E. Riach and R.E. Webber, in *Handbook of Auger Electron Spectroscopy*, 2nd Ed., Physical Electronics Industries Inc., Minnesota, 1976.

[8] H.C. Swart, J.S. Sebastian, T.A. Trottier, S.L. Jones and P.H. Holloway, J. Vac. Sci. Technol., **A 14(3)** (1996) 1697.

[9] S.M. Davidson, J. Microsc., **110** (1977) 177.

Chapter 8

The effect of CdO coating on the degradation of a ZnS thin film phosphor material

8.1. Introduction

Transparent conducting oxide (TCO) thin films have attracted a profound interest for a variety of application in optical, thermal, electronic and solar energy devises. Their high reflectance in the infrared region together with the high transparency in the visible region have been used to make heat mirrors, and the high conductivity has been exploited for the fabrication of highly efficient large-area solar cells [1]. The conductivity and the transparency in the visible region of the TCO material deemed them appropriate for ZnS phosphor film coating. The coating would act as a barrier and reduce surface charging from the virgin phosphor material as the charge can be conducted away [2], reduce desorption of sulphur compounds, lessen the rate of ZnO formation and also transmit the light emitted by the phosphor. Park *et al.* [3] reported a 60% enhancement in the CL efficiency of the ZnS phosphors coated with a thin layer of SiO_2 at voltages below 500 V. They presented a model that attributed the improvement in CL efficiency to a reduction in surface recombination while the decrease in the CL efficiency for thicker coatings was ascribed to electron beam penetration losses in the coating.

Cadmium oxide (CdO) that can be prepared from cadmium nitrate [1,4], cadmium acetate ($Cd(CH_3COO)_2$) [5] and cadmium chloride ($CdCl_2$) [6] salts by a chemical bath deposition technique is one of the cheapest large area methods to coat the phosphor. By this electrodeless chemical deposition method, $Cd(OH)_2$ or $Cd(O_2)_{0.88}(OH)_{0.24}$ thin films are obtained initially, which after annealing are converted into CdO thin films. These films crystallise in the NaCl structure with the same preferential orientation of the as-grown material with high n-type conductivity. Although there are reservations to the application of CdO material due to environmental concerns, CdO films have shown a transmittance of

over 85% in the visible and near infrared region of the spectrum [1,7]. This range accommodates the emission wavelength of the ZnS:Cu,Au,Al emission.

Recent studies conducted on the ZnS:Cu,Au,Al thin film phosphor material, which was degraded in both an O_2 and a CO_2 ambients showed that the thin films degraded according to the ESSCR mechanism [8]. In this chapter the effect of the CdO coated thin film on ZnS:Cu,Au,Al thin films was studied during electron bombardment in an O_2 atmosphere.

8.2. AES, CL, RBS, SEM and XRD analysis

The CdO coating layer was approximately 18 nm thick from the Auger depth profile measurements. The XRD spectrum that was taken on a thicker CdO film that was chemically bath deposited on a glass substrate is shown in Figure 8.1.

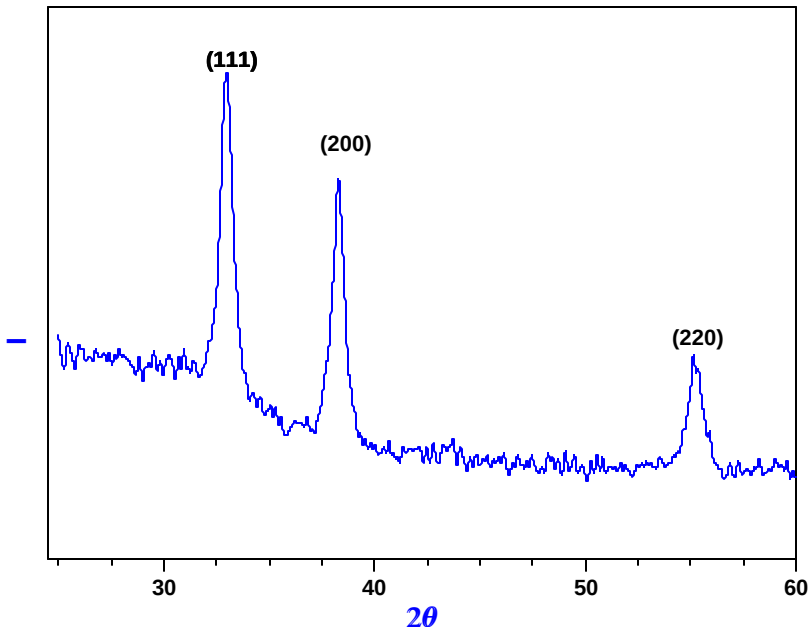

Figure 8.1 XRD spectrum of CdO bulk precipitate on a glass substrate.

This spectrum was also observed by Najdoski *et al.* [4] for the bulk precipitate of CdO.

In Figure 8.2, SEM images of the bare (a) and the coated (b) ZnS:Cu,Au,Al phosphor film are presented. The topography of the surfaces is different indicating a film growth on the surface of the ZnS film that was inserted in the chemical bath for the CdO deposition, Figure 8.2 (b). The thickness of the CdO layer was not uniform on the surface of the phosphor as revealed by the SEM images acquired at different regions of the sample. This should be expected since the chemical bath deposition (CBD) was performed on the surface of the phosphor film that was susceptible to contamination.

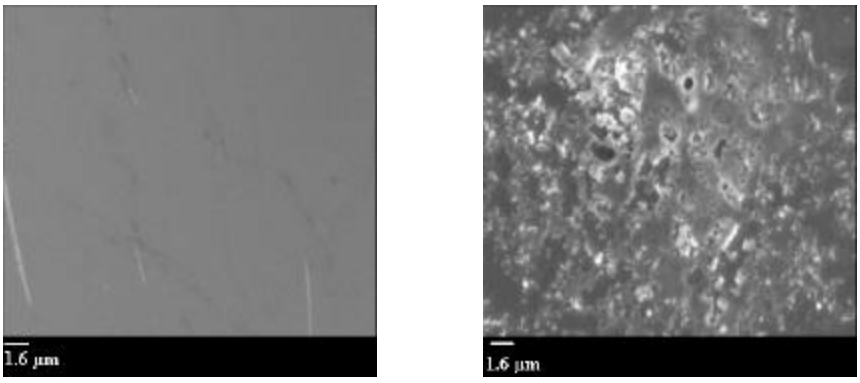

(a) **(b)**

Figure 8.2 SEM images of a ZnS:Cu,Au,Al thin film (a) and a CdO coated ZnS:Cu,Au,Al thin film (b).

Figure 8.3 shows the AES spectra of the CdO coated ZnS:Cu,Au,Al phosphor film, before degradation and after 470 C/cm^2 with 2 keV electron bombardment in 5 x 10^{-7} Torr O_2 ambient. The AES spectrum before degradation reveals S, C, Cl, Cd, O and Zn peaks. The S and Zn were incorporated on the thin film during the CBD or were detected through the holes in the coating. The Cl peak is the residue from the $CdCl_2$ salt used for the CBD and it decreases rapidly with the onset of the electron beam. The Cd and O peaks represent the coating CdO layer. After degradation for 470 C/cm^2 the S, Cl, and C peaks vanish, there is an increase in both the Zn and the O peaks and a decrease in the Cd peak which indicates the formation of ZnO.

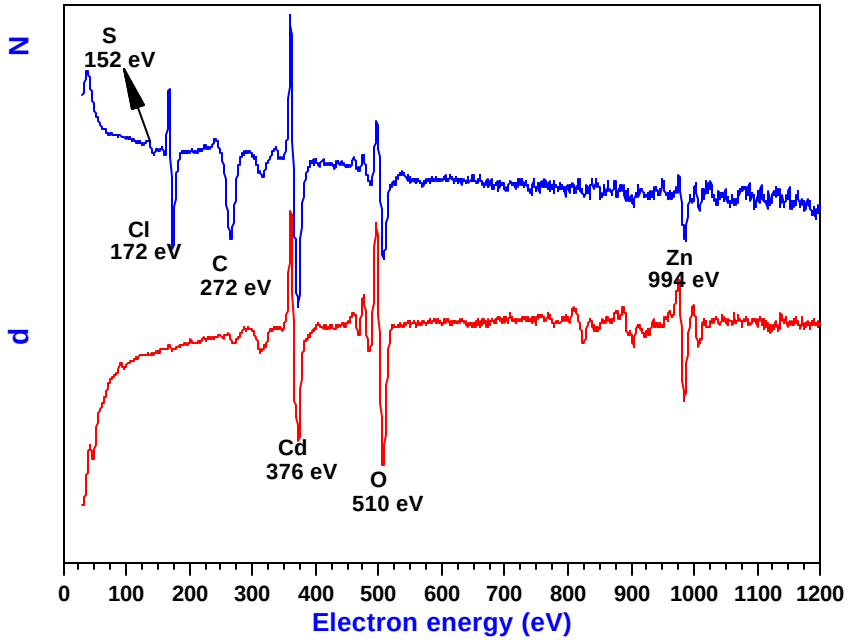

Figure 8.3 Auger spectra before and after degradation in an O_2 ambient for 470 C/cm^2.

Figure 8.4 shows the Auger peak to peak heights (APPHs) of C, Cd, Cl, O, S x 5 and Zn together with the CL intensity against Coulomb dose during electron bombardment in 5 x 10^{-7} Torr O_2 ambient. With the onset of the electron beam the adventitious C and the Cl are depleted from the surface revealing the S, O, Cd and Zn peaks. The O peak is expected to rise as the O_2 molecules that are dissociated to reactive O˙ species by the electron beam [9] constantly impinge the surface. The S peak, which emanates as the C peak is diminishing, decreases after reaching a certain maximum at 100 C/cm^2 until the S is depleted on the surface. There is a significant increase in Zn that starts when the Cd begins to decrease on the surface. There is also a slight decrease in the CL intensity observed, which may be correlated to the surface reactions during the electron beam bombardment. These changes depict that electron beam stimulated surface chemical reactions occurred during electron beam bombardment in an O_2 ambient, resulting in the CL intensity decrease after the reduc tion of Cd on the surface and the formation of ZnO.

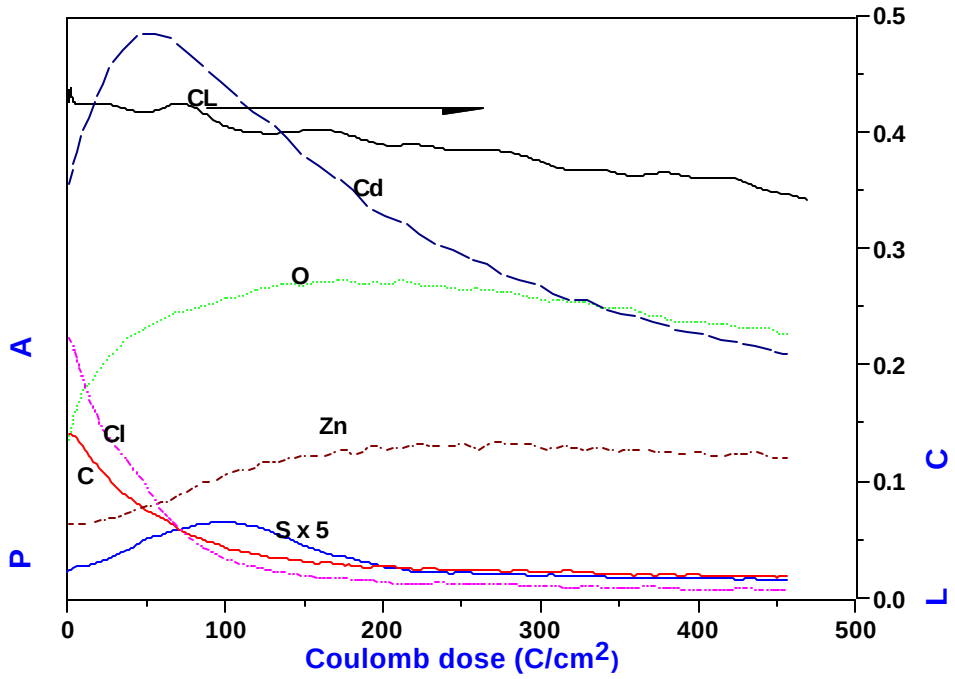

Figure 8.4 APPHs of Cd, O, C, S, Cl and Zn as well as the CL measured during degradation in an O_2 ambient as function of Coulomb dose.

Pospísil and Kusnierik [10] found that the reduction kinetics of CdO-ZnO mixtures depend markedly on the oxides composition. In the CdO-ZnO oxides system irradiated with ^{60}Co gamma rays, the ZnO is non-reducible and the CdO the reducible oxide. Preliminary irradiation of the samples causes an increase in the rate of reduction of samples containing an excess CdO and decrease in the rate of reduction in the region with excess non-reducible ZnO.

The first step in the degradation mechanism is the conversion of the adventitious C into volatile CO_x compounds due to the reactive O^- species resulting from the dissociation of the molecular O_2 by the electron beam. These compounds are then released from the surface. The residual Cl ions are probably converted into oxygen dichloride (Cl_2O) which is also released from the surface. These reactions expose the CdO surface. With further electron beam bombardment an increase in S was measured on the surface. The S forms volatile SO_x compounds with the O^- species on the surface and is soon depleted from the surface. Some studies on electron-beam induced oxidation of CdS [11] revealed no surface compositional changes when 10^{-7} Torr of O_2 was admitted in the analysis chamber

during electron bombardment. Therefore, it is unlikely that CdS was formed on the surface. Lichtensteiger *et al.* [12], also observed the preferential binding of O to S under electron stimulated adsorption of CdS. Therefore, this may imply that S was readily converted to SO_x compounds before any interaction with the Cd as both the S and Cd decrease with electron beam bombardment. The final step involves the reduction of mixed oxides CdO-ZnO that is manifested by an increase in the Zn concentration and a decrease in the Cd concentration.

From the semiconductor point of view both oxides are n-type semiconductors. The n-conduction in CdO results form the presence of Cd^{2+} interstitial and O vacancies acting as donors [13], whereas with ZnO the superstoichiometry of the metal ions is due to the interstitial ions Zn^{+} and Zn^{2+} [10]. When the mixed oxides CdO-ZnO were irradiated at 410 °C with ^{60}Co γ-rays [10], the ionising irradiation lead primarily to the formation of electrons by ionisation processes which resulted in the enhanced reduction of Cd^{2+} ions. With the increasing ZnO content on the surface, the electrons also interacted with the Zn^{+} interstitial probably due to the charge interaction of the two components in close contact. The interstitial Zn^{+} ions of ZnO interact with oxygen vacancies of CdO by the following process:

$$Zn^{+} + |o| \rightarrow Zn^{2+} + e_s^{-} \quad (1)$$

Where $|o|$ is an oxygen vacancy and e_s^{-} is an electron in the vacancy. Electrons with sufficient energy can also raise the conductivity of a semiconductor material based on the redistribution of electrons and holes over existing levels rather than the production or removal of defects [14]. In the case of a prolonged electron beam impact, the electron beam can lead to significant generation of excess free carriers in the proximity of the semiconductor surface [15]. These electrons can then participate in reducing CdO and at low pressures the elemental Cd can easily sublimate. This mechanism is probably responsible for the volatilisation of the Cd and the resulting ZnO on the surface.

Figure 8.5 shows the normalised CL intensity curves against Coulomb dose for the CdO coated (a) and the bare (b) ZnS films up to 370 C/cm^2.

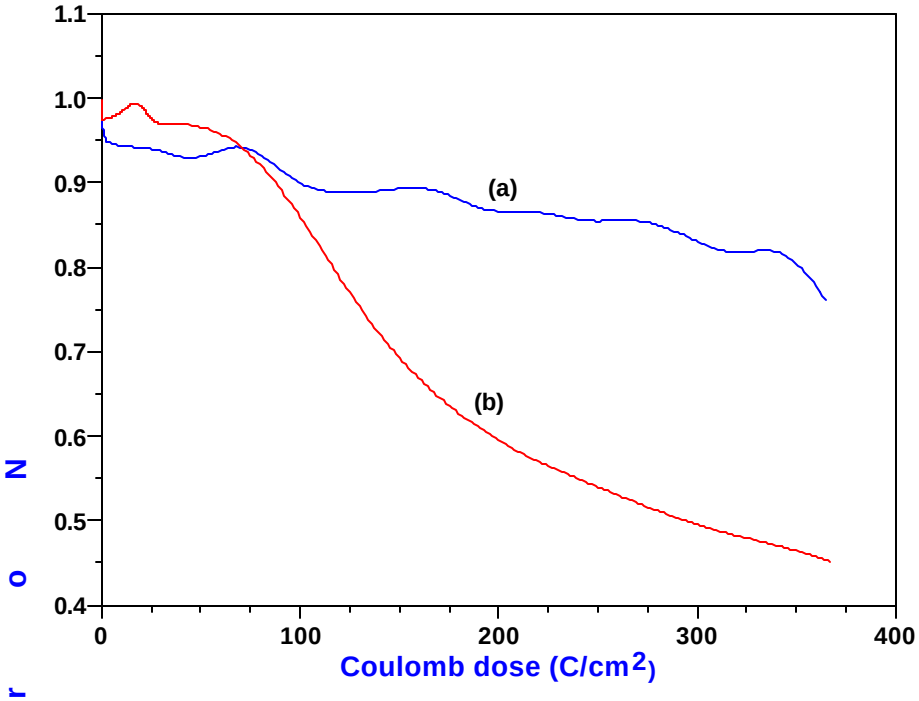

Figure 8.5 Normalised CL intensity measured during degradation for (a) coated and (b) bare ZnS:Cu,Au,Al thin film phosphor as a function of Coulomb dose.

The initial CL for the coated phosphor film was about 50% less than the bare film. The first part of degradation was influenced by the presence of adventitious C on the surface of the films up to ~75 C/cm^2. The CL intensity remained the same until the C was depleted from the surface. This is in agreement with other studies [16] on ZnS phosphor powder, where the onset of CL degradation was after the C was depleted from the surface. As soon as the carbon is depleted the CL for the uncoated ZnS film drastically decreased, Figure 8.5 b. The effect of CdO is evident on the CL curve of the coated sample, Figure 8.6 a. Although there is a decrease in the intensity after the C is depleted, it is not as drastic as compared to the virgin film. This manifest the importance of the barrier formed by the CdO which perforated eventually as the Cd was reduced from the surface.

8.3. Conclusion

The CdO layer was successfully deposited on the ZnS:Cu,Au,Al phosphor film as a transparent conductive oxide barrier by the chemical bath deposition method. The thickness of the CdO film was not uniform throughout the surface coverage. The

degradation mechanism of the CdO coated ZnS film was analysed using AES and CL. Some of the objectives for the CdO coating were accomplished in the sense that the light from the phosphor was transmitted through the CdO layer, the CL stayed constant while the layer was still present and there was no charging observed. The CdO layer, however, decomposed under electron bombardment. The data showed that the degradation was according to the ESSCR mechanism. An electron beam assisted reduction of CdO on the surface was assumed. The CL intensity reduction began after the C was depleted form the surface and the effect of the CdO layer was evident but decreased with the reduction of Cd on the surface.

References:

[1] A.V. Varkey and A.F. Fort, Thin Solid Films, **239** (1994) 211.

[2] H.C. Swart, A.P. Greeff, P.H. Holloway and G.L.P. Berning, Appl. Surf. Sci., **140(1-2)** (1999) 63.

[3] W. Park, B.K. Wagner, G. Russels, K. Yasuda, C.J. Summers, Y.R. Do and H.G. Yang, J. Mater. Res., **15(11)** (2000) 2288.

[4] M.Z. Nadjoski, I.S. Grozdanov and B. Minceva-Sukarova, J. Mater. Chem., **6(5)** (1996) 761.

[5] M. Ocampo, A.M. Fernandez and P.J. Sebastian, Semicond. Sci. Technol. **8** (1993) 750.

[6] M. Ortega-López, A. Morales-Acvedo and Bokhimi, Revista Mexicana de Física **42(5)** (1996) 776.

[7] K. Gurumurugan, D. Mangalaraj, Sa.K. Narayandass and Y. Nakanishi, Mater. Lett., **28** (1996) 307.

[8] K.T. Hillie and H.C. Swart, Appl. Surf. Sci., **183** (2001) 304.

[9] L. Oosthuizen, H.C. Swart, P.E. Viljoen, P.H. Holloway and G.L.P. Berning, Appl. Surf. Sci., **120** (1997) 9.

[10] M. Pospísil and O. Kusnierik, J. Thermal Anal., **25** (1982) 499.

[11] V.B. Mityukhlyaev, Appl. Surf. Sci., **81** (1994) 137.

[12] M. Lichtensteiger, C. Webb and J. Lagowski, Surface Sci., **97** (1980) L375.

[13] K. Gurumurugan, D. Mangalaraj, Sa.K. Narayandass, Y. Nakanishi and Y. Hatanaka, Appl. Surf. Sci., **113/114** (1997) 422.

[14] R.G. Schulze and B.A. Kulp, J. Appl. Phys., 33(7) (1962) 2173.

[15] S.M. Davidson, J. Microscopy **110** (1977) 177.

[16] H.C. Swart, J.S. Sebastian, T.A. Trottier, S.L. Jones and P.H. Holloway, J. Vac. Sci. Technol. **A 14(3)** (1996) 1697.

Chapter 9

Low temperature effect on the degradation of the ZnS phosphor powder

9.1. Introduction

In chapter 5, the effect of annealing on the degradation of the phosphor and consequently the CL was observed. Thermal quenching of the initial luminescence was noticed and explained with the co-ordinate configuration model. The reaction rate at the temperature range (45 °C to 310 °C) was also proven to be controlled by the mean surface stay time of the adsorbed molecule to be dissociated by the electron beam.

This chapter serves as an extension of the temperature studies. The ZnS:Cu,Au,Al phosphor powder was cooled down to –125 °C using liquid nitrogen. AES was used to monitor changes in surface composition during electron bombardment at both room temperature and –125 °C for comparison in 2 x 10^{-6} Torr O_2 ambient. Thermoluminescence (TL) glow curves were attained while the sample was warming up to room temperatures from –125 °C.

9.2. AES and TL analysis

The degradation in all the experiments was according to electron stimulated surface chemical reactions, ESSCR [1,2,3], discussed in Chapter 1.

Figure 9.1 shows the normalised S APPHs acquired at (a) room temperature without the system cooling (see Chapter 3, sec. 3.2.2.), (b) at -125°C without the system being cooled down, (c) at –125 °C with the system cooled down and (d) at room temperature with the system cooled down. The cooling of the vacuum system meant using the liquid nitrogen cryogenic pump.

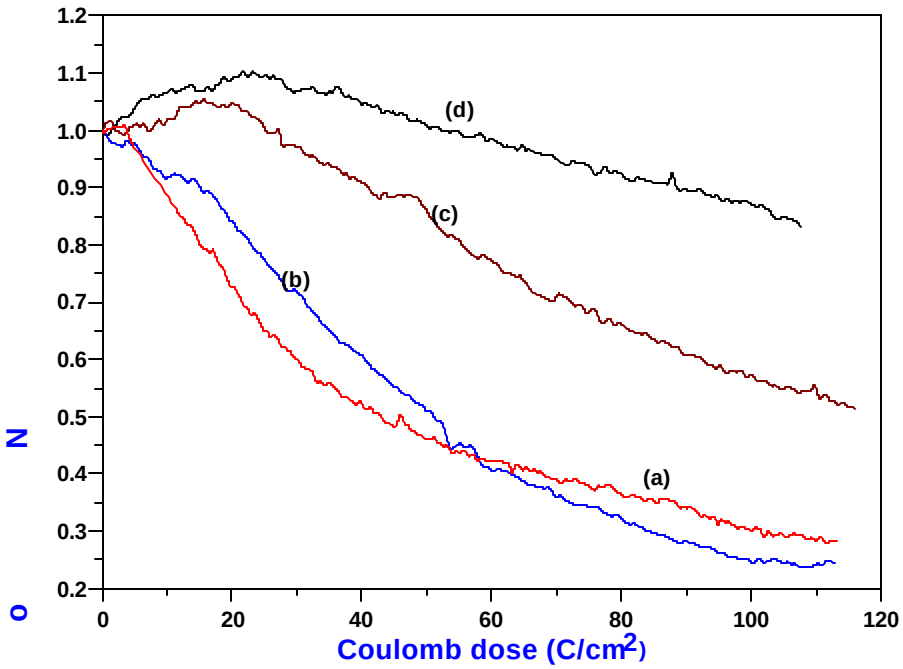

Figure 9.1 Normalised S APPHs as a function of Coulomb dose acquired at (a) room temperature without cooling, (b) at –125 °C without cooling, (c) –125 °C with cooling and (d) room temperature with cooling.

The rate of reaction depicted by the S APPHs at different experimental conditions reveals the influence of the small amount of water vapour that was in the system during electron bombardment. The base pressure was 2.9 x 10^{-9} Torr before back filling with O_2 to 2 x 10^{-6} Torr for all the experiments. At 2.9 x 10^{-9} Torr it was apparent from the RGA that there was still a small amount of water vapour present in the vacuum. The presence of water vapour would increase the rate of degradation of the phosphor [1]. When the phosphor is cooled down using the apparatus shown in Chapter 3 (section. 3.2.2), the stainless steel tubes that were used to introduce liquid nitrogen were bellowed to be flexible as this was required for the experiments. The bellowed tubes had a vast surface area that lead to a large amount of residual water vapour to be frozen on the tubes with the introduction of liquid nitrogen. The water vapour was further reduced when liquid nitrogen was introduced into the system panels, cooling the system. The residual gas analyser revealed that the water vapour peak decreased by 31% from the peak at room temperature when the sample was at –125 °C and by 63% when the vacuum system was also cooled down.

According to the studies of ESSCR at temperatures between 45 and 300 °C, the reaction rate is controlled by the mean surface stay time of the adsorbed molecule on the surface of the phosphor (see Chapter 5). It is then supposed that at low temperatures the rate of reaction will increase, but the influence of the small amount of water vapour at these temperatures is significant. The effect of reduced water vapour competes with the effect of the longer mean surface stay time of the adsorbed molecule at –125 °C (Figure 9.1(b)) and hence a moderate rate of reaction that is comparable with the rate at room temperature (Figure 9.1(a)) both without the cooling of the vacuum system.

Figure 9.1(c) and 9.1 (d) are the S APPHs plotted against the Coulomb dose at –125 °C and at room temperature both with the system cooling, respectively. Both graphs manifest a slower reaction rate proving that the residual water vapour is significantly reduced when liquid nitrogen is introduced into the system panels. The reaction rate at –125 °C (Figure 9.1(c)) is slightly faster than the reaction rate at room temperature (Figure 9.1(d)). This observation substantiates the role of the mean surface stay time of the molecule on the ESSCR, which is longer at lower temperatures and so the relatively increased reaction rate.

TL is the luminescence due to free carriers created by prior irradiation of the sample that are trapped in the band gap structures as they are released from these traps upon increasing temperature to the conduction band and later recombine radiatively. The most suitable method, therefore, to investigate the trap structures introduced by electron bombardment of the phosphor powder is to use TL. During electron beam bombardment in O_2 ambient, O atoms form iso-electronic impurities in the ZnS lattice by substituting for the S atoms [1]. The O atoms have a higher electron affinity than the substituted S atoms and the inclination to attract and trap electrons on these sites will increase. As mentioned in the literature review (Chapter 1), there is a complementary defect theory that is also responsible for the CL degradation.

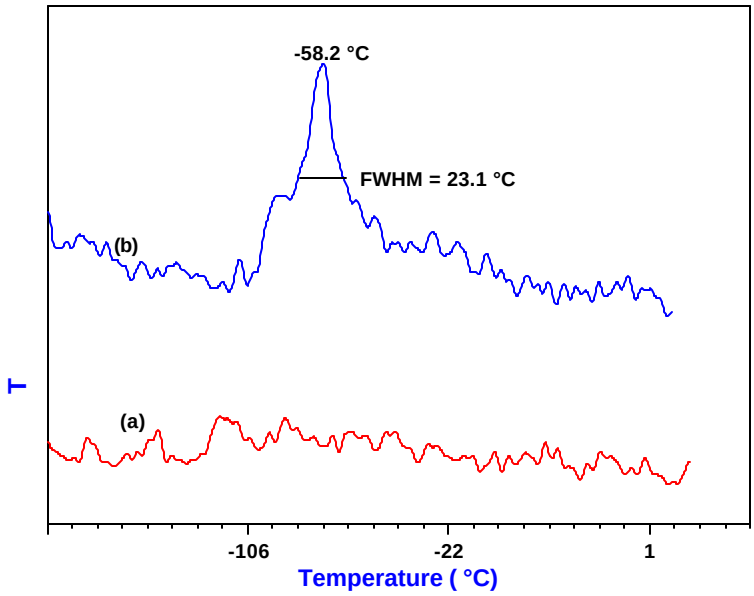

Figure 9.2 TL glow curves of (a) the reference sample and (b) the degraded sample

Figure 9.2 shows the TL glow curves of (a) the reference sample and (b) the degraded sample, which were both bombarded for 20 minutes at –125 °C before acquiring the glow curves. The peak at –58 °C (Figure 9.2 (b)) on the glow curve that was attained after a degraded phosphor powder was cooled down to –125 °C and bombarded for 20 minutes exhibits the effect of O iso-electronic traps. Sebastian [4] also reported the peak at –60 °C attributed to O iso-electronic traps on the TL glow curves acquired on ZnS:Mn phosphor films. It confirms that during the electron bombardment of the ZnS:Cu,Au,Al phosphor powder, O iso-electronic traps were created and they captured free electrons that were excited during the later bombardment at –125 °C. These electrons were then released to the conduction band and later detected as TL as the sample was warming up to room temperature.

The reference sample, Figure 9.2 (a), represents the sample that was just bombarded at –125 °C for 20 minutes without prior degradation. Sebastian [4] observed a peak at –80 °C on the reference ZnS:Mn film, which was attributed to the S interstitial. This peak was not observed on the ZnS:Cu,Au,Al phosphor powder, which means that the S interstitial could have probably resulted from the film growth process [5]. Structural defects such as dislocations and stacking faults formed in the ZnS films have also been reported to seriously affect the CL intensity within a distance of 200 nm from the interface

[6]. Although there is a possible contribution to degradation by some other complex defect [7], however, their effect was not readily observed on the TL glow curves.

9.3. Conclusion

The effect of the mean surface stay time of the absorbed molecule together with the significant influence of the residual water vapour during electron bombardment at low temperatures were verified. The formation of O defects during electron bombardment, which act as electron traps thereby reducing the luminescence efficiency was also confirmed through TL glow curves.

References:

[1] J.S. Sebastian, H.C. Swart, T.A. Trottier, S.L. Jones and P.H. Holloway, J. Vac. Sci. Technol., **A 15(4)** (1997) 1.

[2] H.C. Swart, J.S. Sebastian, T.A. Trottier, S.L. Jones and P.H. Holloway, J. Vac. Sci. Technol., **A 14(3)** (1996) 1697.

[3] L. Oosthuizen, H.C. Swart, P.E. Viljoen, P.H. Holloway and G.L.P. Berning, Appl. Surf. Sci., **120** (1997) 9.

[4] J.S. Sebastian, PhD. Dissertation, University of Florida, Gainesville, FL. 1997.

[5] J. Fang, P.H. Holloway, J.E. Yu, K.S. Jones, B. Pathangey, E. Brettscheneider and T.J. Anderson, Appl. Surf. Sci., **70-71** (1993) 701.

[6] T. Mitsui and N. Yamamoto, Jpn. J. Appl. Phys., **39** (2000) 1172.

[7] Y. Shono and T. Oka, J. Cryst. Growth, **210** (2000) 272.

Chapter 10

Conclusion and recommendations

The degradation of ZnS:Cu,Au,Al phosphor powder and thin films was found to take place by the electron beam stimulated surface chemical reactions that were manifested by the formation of a non-luminescent ZnO layer on the phosphor surface. SO_x and CO_x compounds were also released into the vacuum in the process. The surface reactions correlated with the CL efficiency reduction.

The rate of surface reactions was increased at low current densities due to a longer mean surface stay time of the adsorbed oxygen molecule at lower current densities. Low current densities would also lead to surface charging due to a lower electron conductivity of the phosphor resulting in an increase in the CL degradation rate due to band-bending. A reduced rate of reaction at higher current densities is appreciated, as this will enhance the brightness intensity during operation. The effect of mean surface stay time on the degradation of the phosphor was also observed on annealing the sample between 45 °C and 300 °C resulting in an increased reaction rate at lower temperatures. The role of local heating on the reactions at temperatures between 45 °C and 300 °C was ruled out as the reactions did not continue at the intervals when the electron beam was switched off during the experiments at higher temperatures. Thermal quenching of the CL is also significant at higher temperatures.

At low temperatures the rate of degradation was accelerated, which is in agreement with the above explanation. The residual water vapour in the vacuum highly influenced the degradation rate, as it was frozen at low temperatures, this resulted in a moderate rate at – 125 °C that was comparable to the rate at room temperature. The formation of O defects during electron bombardment, which act as electron traps was also confirmed through TL glow curves as the degraded phosphor was warming up to room temperature from –125 °C.

Thin films of ZnS phosphor material were also successfully deposited on Si (100) by using pulsed laser deposition method. The effect of the N_2 gas that was introduced into the vacuum chamber during deposition was evident on the growth rate of the thin films. N_2 gas was introduced to modify the energetic ablated plasma plume during deposition. The films were emitting and they were used for degradation studies in both the O_2 and CO_2 ambients. Degradation in the CO_2 ambient was less severe than in O_2 due to the partial deposition of C on the phosphor surface during degradation in CO_2.

To provide a barrier for the phosphor film degradation, which will also transmit light and conduct, transparent conducting oxides (TCO) were considered. A thin layer of CdO was deposited on the ZnS thin film using chemical bath deposition (CBD) for this purpose. The CdO layer transmitted the emitted light by the phosphor, there was no charging experienced and the CL intensity stayed constant until the layer decomposed due to the reduction of Cd.

The compatibility of the ZnS:Cu,Au,Al phosphor in the FED environment can be achieved if the release of SO_x compounds can be drastically reduced as these may poison the emitter tips. The rate at which these compounds are released principally depends on the residual gas species in the vacuum. It is difficult to eliminate all these gas species in the high surface to volume ratio associated with the FED environment without drastically altering the technology.

Carbon deposition on the surface of the phosphor by cracking hydrocarbons or by the dissociation of CO_x molecules can be one solution as degradation only commences after the adventitious C is depleted on the surface.

The transparent conducting oxide (TCO) coating of the phosphor is another appealing solution as it drastically reduces the release of S compounds and delays the formation of the non-luminescent ZnO layer. There are a number of candidate TCO materials that can still be investigated as barriers for the degradation reactions. Although, superior TCO

properties like high mobility and reduced resistance are possessed by cadmium compounds, concerns about its toxicity can not be ignored.

Pulsed excimer laser deposition (PLD) of thin films proved to be a carbon free physical deposition method that also retains stiochiometry. Thin film phosphors provide less degassing and a superior screen thermal contact but their CL efficiency is still very low compared to powdered phosphors. However, thin films are more appropriate for film coating investigations due to the near homogeneous surface structure. In future studies SnO_2 and indium doped SnO_2 (ITO) that are transmitting in the visible to near infrared will be deposited on the ZnS films as TCO barrier materials. ZnS:Cu,Au,Al thin film phosphors and the TCO coating materials will be deposited using PLD method.

The role of defects on the degradation of the phosphor is also evident. The O substitutional atoms that act as the electron trap were revealed by the TL glow curves. The effect of these traps was also observed on ZnS:Mn thin film phosphors. It was interesting to note that the peak due to the S interstitial observed on the ZnS:Mn thin film was not detected on the reference-powdered phosphor material. Defects and the stacking faults are inherent to the thin film deposition process. Dislocations and stacking faults formed in the ZnS films were reported to seriously affect the CL intensity within a distance of 200 nm from the interface. Another batch of ZnS:Cu,Au,Al phosphor films will also be used for future experiments to study the role of defects on the degradation of the phosphor instead of the powder material. Studies aimed at quantifying the effect caused by the defects will also be embarked on. Deep level transient spectroscopy (DLTS) will also be used as a complementary technique in these experiments.

The overall studies showed that ZnS phosphor material still maintains high efficiency even at high residual gas pressures and low electron beam energies associated with the FED environment. The efficiency of the near surface generated CL due to low electron beam energies in the FED environment is significantly affected by the surface state of the phosphor material. Electron beam bombardment introduced defects also affect the CL

degradation. As mentioned in the above text, there are continuing investigations to minimise the effect of impinging reactive residual species on the surface of the phosphor material during operation. If these problems can be thoroughly addressed, ZnS:Cu,Au,Al phosphor will be a vital part of the FED technology in the future.

APPENDIX

Calculations to predict the spontaneity of the reactions at any temperature by using the Gibbs-Helmholtz equation*:

Reaction:

$$ZnS + 2O_2 \rightarrow ZnO + SO_3$$

For: ZnS

$\Delta H°_f$ = - 49.23 kcal/mol

$S°$ = 13.8 eu

ZnO

$\Delta H°_f$ = - 83.24 kcal/mol

$S°$ = 10.43 eu

For: O_2

$\Delta H°_f$ = 0 kcal/mol

$S°$ = 49.003 eu

SO_3

$\Delta H°_f$ = - 94.58 kcal/mol

$S°$ = 61.34 eu

The enthalpy (ΔH) of the reaction at 25°C:

$$\Delta H = [\Delta H°_f(ZnO) + \Delta H°_f(SO_3)]_{products} - [\Delta H°_f(ZnS) + \Delta H°_f(2O_2)]_{reactants}$$
$$= [(-83.24) + (-94.58)] - [(-49.23) - (2 \times 0)]$$
$$= - 128.59 \text{ kcal/mol}$$

The entropy (ΔS) of the reaction at 25°C:

$$\Delta S = [(S°(ZnO) + S°(SO_3)]_{products} - [S°(ZnS) + S°(2O_2)]_{reactants}$$
$$= [10.43 + 61.34] - [13.8 + (2 \times 49.003)]$$
$$= - 40.04 \text{ eu}$$

To predict the temperature when $\Delta G = 0$:

$$T = \Delta H/\Delta S$$
$$= -128590 \text{ cal}/- 40.036 \text{ cal per °K}$$
$$= 3211.54 \text{ °K}$$
$$= 2938.54 \text{ °C}$$

Therefore the reaction will be spontaneously above 2938 °C.

Reaction:

$$2ZnS + 3O_2 \rightarrow 2ZnO + 2SO_2$$

For: ZnS

$\Delta H°_f$ = - 49.23 kcal/mol

$S°$ = 13.8 eu

ZnO

$\Delta H°_f$ = - 83.24 kcal/mol

$S°$ = 10.43 eu

For: O_2

$\Delta H°_f$ = 0 kcal/mol

$S°$ = 49.003 eu

SO_2

$\Delta H°_f$ = - 70.994 kcal/mol

$S°$ = 59.30 eu

The enthalpy (ΔH) of the reaction at 25°C:

$$\Delta H = [\Delta H°_f(2ZnO) + \Delta H°_f(2SO_2)]_{products} - [\Delta H°_f(2ZnS) + \Delta H°_f(3O_2)]_{reactants}$$
$$= [(2 \times -83.24) + (2 \times -70.994)] - [(2 \times -49.23) - (3 \times 0)]$$
$$= - 210.008 \text{ kcal/mol}$$

The entropy (ΔS) of the reaction at 25°C:

$$\Delta S = [(S°(2ZnO) + S°(2SO_2)]_{products} - [S°(2ZnS) + S°(3O_2)]_{reactants}$$
$$= [2 \times 10.43 + 2 \times 59.30] - [2 \times 13.8 + (3 \times 49.003)]$$
$$= - 35.15 \text{ eu}$$

To predict the temperature when $\Delta G = 0$:

$$T = \Delta H/\Delta S$$
$$= -210008 \text{ cal}/- 35.15 \text{ cal per °K}$$
$$= 5974.62 \text{ °K}$$
$$= 5701.62 \text{ °C}$$

Therefore the reaction will be spontaneously above 5701 °C.

* E.R. Toon, G.L. Ellis and J. Brodkin, *In Foundations of Chemistry* (Ed. Holt, Rinehart and Winston, Inc. New York), 1968, p 386.

LIST OF FIGURES

Figure 1.1 (p. 3) shows the cross-sectional view of the field emission cathodes (FED)
Figure 2.1 (p. 12) shows models of electron transitions resulting in luminescence
Figure 2.2 (p. 13) shows the schematic presentation of the luminescence process in ZnS:Cu,Al,Au phosphor
Figure 2.3 (p. 18) shows the configuration co-ordinate model of a luminescent centre
Figure 3.1 (p. 29) shows the cross sectional schematics of the heating (a) and cooling (b) set-ups.
Figure 4.1 (p. 36) shows the APPHs of S, C, O and Zn as well as the CL measured at a current density of 88 mA cm^{-2} as a function of Coulomb dose.
Figure 4.2 (p. 37) shows the APPHs of S, C, O and Zn as well as the CL measured at a current density of 2.5 mA cm^{-2} as a function of Coulomb dose.
Figure 4.3 (p. 37) shows the normalised APPHs of sulphur at different electron current densities as a function of Coulomb dose.
Figure 4.4 (p. 39) shows the normalised CL intensities measured at different electron current densities as a function of Coulomb dose.
Figure 5.1 (p. 44) shows the APPHs of S, C x 5, O and Zn as well as the CL as a function of Coulomb dose measured at a current density of 88 mA/cm^2 at temperatures of (a) 46 °C, (b) 200 °C and (c) 300 °C as indicated.
Figure 5.2 (p. 45) shows the CL intensity as function of temperature at a pressure of 2 x 10^{-9} Torr before any degradation.
Figure 5.3 (p. 46-47) shows the APPHs of S, O and Zn as function of Coulomb dose measured at a current density of 88 mA/cm^2 at temperatures of (a) 48 °C and (b) 310 °C as indicated. (c) At 210°C shows the S APPHs of a continuous e-beam bombardment and of a bombardment with e-beam shut off intervals, after sputtering.
Figure 5.4 (p. 48) shows the Coulomb doses required to reach 60% of the original S signal as function of temperature
Figure 6.1 (p. 54) shows the RBS spectrum of pulsed laser deposited ZnS phosphor film on Si (100), the dotted line is the ZnS 1:1 compositional simulation.
Figure 6.2 (p. 55) shows the AES differential energy spectra of (a) first layer before sputtering, (b) sample 1 and (c) sample 4, both during sputtering.
Figure 6.3 (p. 56) shows the AES depth profiles of (a) sample 1 and (b) sample 4
Figure 6.4 (p. 56) shows three dimensional AFM images of the ZnS films deposited on Si (100), (a) Sample 1 and (b) Sample 4.
Figure 6.5 (p. 57) shows the statistical presentation of calculated rms roughness (R_{rms}) values for all the films.
Figure 6.6 (p. 58) shows the film thickness values from the RBS measurements
Figure 6.7 (p. 59) shows XRD spectra of the films, (a) sample 1, (b) sample 2, (c) sample 3 and (d) sample 4. (e) Is a spectrum of the target material.
Figure 7.1 (p. 63) shows AES differential energy spectra of (a) film before degradation, (b) and (c) film after degradation for a Coulomb dose of about 300 C/cm^2 in O_2 and CO_2, respectively.
Figure 7.2 (p. 64) shows the APPHs of S, C, O, and Zn as well as the CL measured during degradation in an O_2 ambient (a) and a CO_2 ambient (b).
Figure 7.3 (p. 66) shows the normalised APPH of sulphur for different electron beam energies as a function of Coulomb dose.
Figure 7.4 (p. 67) shows the CL intensity at different electron beam energies
Figure 8.1 (p. 70) shows the XRD spectrum of CdO bulk precipitate on a glass substrate.
Figure 8.2 (p. 71) shows SEM images of a ZnS:Cu,Au,Al thin film (a) and a CdO coated ZnS:Cu,Au,Al thin film (b).
Figure 8.3 (p. 72) shows Auger spectra before and after degradation in an O_2 ambient for 470 C/cm^2.
Figure 8.4 (p. 73) shows APPHs of Cd, O, C, S, Cl and Zn as well as the CL measured during degradation in an O_2 ambient as function of Coulomb dose
Figure 8.5 (p. 75) shows the normalised CL intensity measured during degradation for (a) coated and (b) bare ZnS:Cu,Au,Al thin film phosphor as a function of Coulomb dose.
Figure 9.1 (p. 79) shows the normalised S APPHs as a function of Coulomb dose acquired at (a) room temperature without cooling, (b) at −125 °C without cooling, (c) −125 °C with cooling and (d) room temperature with cooling.
Figure 9.2 (p. 81) shows the TL glow curves of (a) the reference sample and (b) the degraded sample.

BIBLIOGRAPHY

Degrees:

BSc, BSc Hons, MSc (cum laude)

Presentations in international conferences:

1. The Growth of Cu films on SiO_2 by atmospheric pressure Metalorganic Vapour Phase Epitaxy (MOVPE) at the Sixth European Workshop on Metal -Organic vapour phase epitaxy and related growth techniques. Gent, Belgium June 1995.
G. Scriven, *K.T.Hillie*, A. Leitch, V.V.Kozyrkov and C.M.Demanet

2. Investigation of various deaning procedures of transparent conducting oxide substrate for CdS/CdTe photovoltaic cells using Scanning Force Microscopy.
Presented at the Fourth Workshop on Industrial Applications of Scanned Probe Microscopy, Gaithersburg (Md), 6-8 May 1997.
C.M. Demanet, *K.T. Hillie*, J.M. Nel, F.D. Auret and H.L.Gaigher

3. AFM, LFM and Force Modulation assessment of cleaning procedures on metal oxide on glass substrate for photovoltaic applications, at the 7th European Conference on Applications of Surface and Interface Analysis, Gothenborg, Sweden. 16-20 June 1997.
K.T. Hillie, C.M. Demanet, J.M. Nel and F.D. Auret

4. Effect of Cleaning Procedures on the Quality of Palladium Schottky Barrier Diodes Fabricated on Epitaxially Grown n-Si, at the 7th European Conference on Applications of Surface and Interface Analysis, Gothenborg, Sweden 16-20 June 1997.
K.T. Hillie, C.M. Demanet, P.N.K. Deenapanray, F.D.Auret and G. Myburg

5. Degradation of FED phosphors. At the 8th European Conference on Applications of Surface and Interface Analysis, Sevilla, Spain 4-8 October 1999.
H.C. Swart and *K.T. Hillie*

6. On the degradation of ZnS:Cu,Al,Au phosphor powder: the effects of temperature, 14th International Conference on Defects in Insulating Materials (ICDM), Johannesburg-Midrand, South Africa 3-7 April 2000.
K.T. Hillie and H.C. Swart

7. The effect of temperature on the degradation of ZnS FED phosphors, presented at APSIAC'2000, Beijing, China 2000.
H.C. Swart, *K.T. Hillie* and A.P. Greeff.

Presentations in local conferences:

1. Experimental determination of the shape and radius of Atomic Force Microscope tips.
July 1994 at the SAIP* Annual Conference in Mmabatho RSA.
K.T. Hillie and C.M.Demanet

2. Atomic Force Microscope Investigation of Chemical Vapour Deposited Cu film on SiO_2 (June 1995) At the SAIP* annual Conference in Cape Town RSA.
K.T. Hillie and C.M.Demanet.

3. Scanning Force Microscope investigation of various methods of cleaning conducting oxide substrates on glass for photovoltaic cell. July 1996 at the Annual SAIP* Conference in Pretoria RSA.
K.T.Hillie, C.M. Demanet, J.M. Nel and F.D Auret

4. AFM characterisation of the morphological properties of the chalchopyrites $CuInSe_2$ and $Cu(In,Ga)Se_2$ absorber layers for photovoltaic applications. At the annual SAIP* conference in Cape Town, July 1998.
K.T. Hillie, C.M. Demanet, and V.Alberts.

5. The effect of current density on the degradation of ZnS:Cu,Al,Au phosphor powders under electron bombardment. At the annual SAIP* conference in Port Elizabeth, 03-09 July 1999.
K.T. Hillie, G.L.P. Berning and H.C. Swart

6. Influence of Substrate morphology and temperature on Electrodeposited CdS thin films. At the SAIP* annual conference in Port Elizabeth RSA, 1999.
J.M. Nel, M. van Staden, G. Myburg, *K.T. Hillie*, C.M. Demanet, C.W. Louw, H.L.Gaigher and F.D. Auret.

7. The effect of temperature on the degradation of ZnS FED phosphors. At the annual SAIP* conference in Johannesburg, July 2000.
K.T. Hillie, H.C. Swart, and A.P. Greeff

8. ZnS thin films grown on Si(100) by XeCl pulsed laser ablation. At the annual SAIP* conference in Johannesburg, July 2000.
K.T. Hillie and H.C. Swart.

9. Electron beam induced degradation of a ZnS:Cu,Au,Al thin film phosphor on Si(100) substrate, At the annual SAIP* conference in Durban, July 2001.
K.T. Hillie and H.C. Swart

SAIP* - South African Institute of Physics

Manuscripts appearing in conference proceedings:

1. The Growth of Cu films on SiO_2 by atmospheric pressure Metalorganic Vapour Phase Epitaxy (MOVPE). Workshop Booklet. EW MOVPE VI. 6th European Workshop on Metal Organic Vapour Phase Epitaxy and Related Growth Techniques, A 20, 1995.
G. Scriven, *K.T.Hillie*, A. Leitch V.V.Kozyrkov and C.M.Demanet

2. Effect of Cleaning Procedures on the Quality of Palladium Schottky Barrier Diodes Fabricated on Epitaxially Grown n-Si. Proceedings of the 7th European Conference on Applications of Surface and Interface Analysis (ECASIA'97), p511, 1997.
K.T. Hillie, C.M. Demanet, P.N.K. Deenapanray, F.D. Auret, G. Myburg.

3. AFM, LFM and Force Modulation assessment of cleaning procedures on metal oxide on glass substrate for photovoltaic applications. Proceedings of the 7th European Conference on Applications of Surface and Interface Analysis (ECASIA'97), p583, 1997.
K.T. Hillie, C.M. Demanet, J.M. Nel, F.D. Auret.

4. Characterisation of polycrystalline $CuInSe_2$ thin films by atomic force microscopy imaging. Proceedings of the 37th Annual Conference of the Microscopy Society of Southern Africa (MSSA), **29**, 1998.
V. Alberts, *K.T. Hillie* and C.M. Demanet.

Publications in international Journals:

1. Using scanning force microscopy (SFM) to investigate cleaning procedures of different transparent conducting oxide substrates. Applied Surface Science, **134,** 22-30, 1998.
J.M. Nel, *K.T. Hillie*, C.M.Demanet, F.D. Auret and H.L. Gaigher

2. Atomic Force Microscopy Study of Si(111) Surface Morphology and Electrical Characteristics of Pd/n-Si Schottky Diodes: Effect of Cleaning Procedures. Surface and Interface analysis, **26**, 748-757, 1998.
P.N.K. Deenapanray, *K.T. Hillie*, F.D. Auret, G.Myburg and C.M. Demanet.

3. Atomic Force Microscopy and High-resolution RBS Investigation of the Surface Modification of Magnetron Sputter-etched Si(111) in an Argon Plasma at Different Pressures. Surface and Interface analysis, **27**, 881-888, 1999.
P.N.K. Deenapanray, *K.T. Hillie*, C.M. Demanet and M.C. Ridgway.

4. Degradation of ZnS FED Phosphors. Surface and Interface Analysis, **30**, 383, 2000.
H.C. Swart and *K.T. Hillie*.

5. Atomic force microscopy imaging of polycrystalline $CuInSe_2$ thin films. Journal of Microscopy-Oxford, **197**, 206-215, 2000.
V. Alberts, *K.T. Hillie* and C.M. Demanet

6. On the degradation of ZnS:Cu,Al,Au phosphor powder: The effects of temperature,
Radiation Effects and Defects in Solids, **154 (3-4)**, 373-376, 2001**.**
K.T. Hillie and H.C. Swart

7. ZnS thin films grown on Si(100) by XeCl pulsed laser ablation. Applied Surface Science, **177 (1-2)**, 73-77, 2001.
K.T. Hillie, C. Curren and H.C. Swart

8. The effect of temperature on the degradation of ZnS FED phosphors. Surface and Interface Analysis, **32**, 110-113, 2001.
H.C. Swart, *K.T. Hillie* and A.P. Greeff

9. Electron beam induced degradation of a pulsed laser deposited ZnS:Cu,Au,Al thin film on a Si(100) substrate. Applied Surface Science, **183,** 304-307**,** 2001.
K.T. Hillie and H.C. Swart

10. Effect of a CdO coating on the degradation of a ZnS thin film phosphor material. Applied Surface Science. **187**, 139-146, 2002.
K.T. Hillie, S.S. Basson and H.C. Swart

11. Low temperature effect on the electron beam induced degradation of ZnS:Cu,Au,Al phosphor powders Applied Surface Science. Submitted.
K.T. Hillie and H.C. Swart